~~Methane~~Sea-air methane flux estimates derived from continuous atmospheric measurements and ~~surface-water observations~~marine depth profiles in ~~the northern Labrador Sea and Baffin Bay~~cold seep regions

Judith Vogt[1,2], David Risk[1], Evelise Bourlon[1], Kumiko Azetsu-Scott[3], Evan N. Edinger[4], Owen A. Sherwood[5]

[1]Department of Earth Sciences, St. Francis Xavier University, Antigonish, B2G2W5, Canada
[2]Environmental Science Program, Memorial University of Newfoundland, St. John's, A1B3X7, Canada
[3]~~DFisheries~~Fisheries and Oceans, Bedford Institute of Oceanography, Dartmouth, B2Y4A2, Canada
[4]Department of Geography, Memorial University of Newfoundland, St. John's, A1B3X9, Canada
[5]Department of Earth and Environmental Sciences, Dalhousie University, Halifax, B3H4R2, Canada

Correspondence to: Judith Vogt (jvogt@mun.ca)

Abstract. Vast amounts of methane (CH_4) stored in ~~permafrost and~~ submarine sediments are susceptible to release in a warming Arctic, further exacerbating climate change in a positive feedback. It is therefore critical to monitor CH_4 over pan-regional scales to detect early signs of CH_4 release. However, our ability to monitor CH_4 is hampered in remote northern regions by sampling and logistical constraints and few good baseline data exist in many areas. ~~To create~~From high-resolution atmospheric CH_4 measurements and discrete surface water samples, we estimated instantaneous sea-air CH_4 fluxes at various locations. We also created a baseline study of current background levels of CH_4 in North Atlantic waters~~, we collected continuous real-time~~ based on the atmospheric CH_4 data~~, along with ambient air temperature and wind parameters~~ over 22 days in summer 2021 on a roughly 5100 km voyage in the northern Labrador Sea and Baffin Bay ~~up to 71~~between 55 °N and 72 °N. In addition, we measured CH_4 concentrations ~~in~~across the water column ~~using discrete water samples~~ at ~~selected~~various stations. Measured atmospheric mixing ratios of CH_4 ranged from 1944~~.7 ppb~~ ppbv to 2012~~.0 ppb~~ ppbv, with a mean of 1966~~.0±7.4 ppb~~±8 ppbv and a baseline of 1954~~.2–1980.6 ppb.~~–1981 ppbv. Dissolved CH_4 concentrations in the near-surface water peaked at ~~56.58±0.05 nM~~5.3 nmol/L within 1 km down-current of a known cold seep at Scott Inlet ~~but~~and were consistently ~~super-saturated~~oversaturated throughout the water column in Southwind Fjord, which is an area recently affected by submarine landslides. Local sea-air CH_4 fluxes ranged from 0.~~1–14.1~~003–0.119 µmol m^{-2} d^{-1} indicating that the ocean ~~acted as a~~released only small amounts of CH_4 ~~source~~ to the atmosphere~~.~~ at all stations. Atmospheric CH_4 levels were also driven by meteorological, spatial, and temporal variations~~. Highest atmospheric CH_4 mixing ratios were detected in the Cumberland Sound in Nunavut, suggesting~~, and both onshore ~~sources from nearby waterbodies and wetlands, whereas~~and ocean-based contributions ~~at this location could not be ruled out.~~to atmospheric CH_4 mixing ratios are likely. Coupled ~~real-time~~high-resolution measurements of marine and atmospheric CH_4 data have the potential to provide ongoing monitoring in a region susceptible to CH_4 releases, as well as critical validation data for global-scale measurements and modelling.

1 Introduction

Global atmospheric methane (CH_4) levels have substantially increased in recent years, with the largest recorded yearly increase from 2020 to 2021 ~~(Dlugokencky, 2016; Nisbet et al., 2019). Due to the high radiative activity of the greenhouse gas CH_4, close observations of atmospheric levels are needed to determine trends and impacts on the future climate. While Arctic regions are subject to rapid warming~~ (Dlugokencky, 2016; Nisbet et al., 2019). Due to the high radiative forcing of the greenhouse gas CH_4, close observations of atmospheric levels are needed to immediately detect trends and impacts on the future climate. While Arctic regions are subject to rapid warming (Meredith et al., 2019)~~, measurements of atmospheric CH_4 levels in these regions are scarce, especially over the ocean. The Arctic Ocean contains large amounts of CH_4 in sediments along the continental margins. With ongoing climate change, permafrost thaw, destabilization of CH_4 hydrates and reduction of sea ice cover may make the Arctic Ocean susceptible to substantial CH_4 release further exacerbating global warming (James et al., 2016). Seafloor gas seeps releasing CH_4-rich bubbles into the water column are often found along continental margins. However, the contribution of seafloor gas seeps to atmospheric CH_4 entails large uncertainties (Saunois et al., 2016), mostly due to significant temporal and spatial differences of emissions (Boles et al., 2001; Leifer and Boles, 2005; Shakhova et al., 2014; Cramm et al., 2021; Dølven et al., 2022). Water depth and the abundance of methanotrophic bacteria influence the oxidation of CH_4, and the speed and strength of currents affects the dissolution of the gas (McGinnis et al., 2006; Reeburgh, 2007; Leonte et al., 2017; Silyakova et al., 2020). Among others, these factors determine how much of the gas diffuses~~, measurements of atmospheric CH_4 levels in these regions are scarce, especially over the ocean. The Arctic Ocean contains large amounts of CH_4 in sediments along the continental margins (Kvenvolden, 1988; Shakhova et al., 2010; Mau et al., 2017). With ongoing climate change, permafrost thaw, destabilization of CH_4 hydrates and reduction of sea ice cover may make the Arctic Ocean susceptible to substantial CH_4 release further exacerbating global warming (James et al., 2016). Seafloor gas seeps releasing CH_4-rich bubbles into the water column are often found along continental margins. However, the contribution of seafloor gas seeps to atmospheric CH_4 entails large uncertainties (Saunois et al., 2016), mostly due to significant temporal and spatial differences of emissions (Boles et al., 2001; Leifer and Boles, 2005; Shakhova et al., 2014; Cramm et al., 2021; Dølven et al., 2022). Water depth and the abundance of methanotrophic bacteria influence the oxidation of CH_4, and the speed and strength of currents affect the distribution of the gas in surface waters and in the water column (McGinnis et al., 2006; Reeburgh, 2007; Leonte et al., 2017; Silyakova et al., 2020). Among others, these factors determine how much of the gas escapes to the atmosphere.

While the East Siberian Arctic Shelf overall releases up to 4.5 Tg CH_4 yr^{-1} ~~of CH_4~~ of mostly thermogenic, but also biogenic origin (Berchet et al., 2020) with large temporal and spatial variability ~~(Shakhova et al., 2010, 2014; Thornton et al., 2016, 2020)~~(Shakhova et al., 2010, 2014; Thornton et al., 2016, 2020), prevailing thought suggests that the North American Arctic Ocean contributes relatively little CH_4 to the atmosphere (Manning et al., 2022). Increasing atmospheric concentrations of CH_4 have however been reported over the European Arctic Ocean and mostly attributed to land-based sources, but also marine point- sources from active underwater seeps (Platt et al., 2018). While a few studies focused on dissolved CH_4 levels in ~~north-eastern~~northeastern Canadian Arctic waters (Punshon et al., 2014, 2019) where seep locations were suggested (Jauer and

Budkewitsch, 2010; Punshon et al., 2019) or confirmed (Cramm et al., 2021), continuous measurements of atmospheric CH_4 levels in this region are lacking and more measurements in this area are needed. To investigate how the identified seep areas affected atmospheric CH_4 levels, we conducted ~~mobile~~ CH_4 monitoring onboard the icebreaker CCGS *Amundsen*. We collected measurements of CH_4 dissolved in the water column at ~~select~~various locations between the northern Labrador Sea to Baffin Bay adding to a small but growing body of data on water column CH_4 concentrations in the Arctic and sub-Arctic seas. We also tracked atmospheric CH_4 levels continuously along a north-south transect to establish a baseline study for above-ocean CH_4 mixing ratios in the area that can be used as a benchmark for further monitoring of CH_4 levels in Arctic regions.

2 Methods

2.1 Study area

Data for this study was collected during an expedition of the Canadian research icebreaker CCGS *Amundsen* starting on July 15, 2021, in St. John's, Newfoundland, Canada, and ending on August 12, 2021, in Iqaluit, Nunavut, Canada. The expedition transited the western Labrador Sea, Davis Strait, and Baffin Bay along the ~~north-eastern~~northeastern Canadian continental shelf (Fig. 1). Along the shelf margins, seafloor gas seepage was previously localized at Scott Inlet, Baffin Bay (71~~.37812~~° 22' 41.2" N, ~~-~~70~~.07452~~° 04' 28.3" W) (Loncarevic and Falconer, 1977; Levy and MacIean, 1981; Cramm et al., 2021), while further locations were suggested in the Saglek Basin in northern Labrador (60~~.351~~° 21' 03.6" N, ~~-~~61~~.864~~° 51' 50.4" W) (Jauer and Budkewitsch, 2010; Punshon et al., 2019) and off the coast of Cape Dyer, Baffin Island (67~~.449~~° 26' 56.4" N, ~~-~~61~~.919~~° 55' 08.4" W) (Punshon et al., 2019)~~.~~ also indicated in Figure 1. The studied region lies within the seasonal sea ice zone and ~~the ocean was partially covered with~~partial sea ice cover was observed in the northernmost regions~~.~~ between July 30, 2021, and August 3, 2021. Hydrography in the studied area is dominated by the Baffin Island Current (BIC~~). The BIC is~~), the integrated Arctic outflow through the Canadian Arctic Archipelago~~, flowing~~. The BIC flows southward along the Baffin Island coast and slope~~. The BIC~~ and becomes a component of the Labrador Current~~,~~ (Fig. 1), being modified by the Hudson Strait overflow, and continues flowing southward, mainly confined to the shelf and upper slope (Azetsu-Scott et al., 2012). The West Greenland Current bifurcates at Davis Strait, with part of the flow entering Baffin Bay on the eastern side of Davis Strait and contributing to the cyclonic circulation in the Bay, and partly continuing westward as the Labrador Sea cyclonic circulation (Melling et al., 2001; Tang et al., 2004; Wu et al., 2013). The eastern coast of Baffin Island is characterized by the Baffin Mountains, with elevations up to 2147 m. With its location north of the tree line, the land is dominantly barren and sparsely vegetated, or covered with smaller waterbodies and wetland areas.

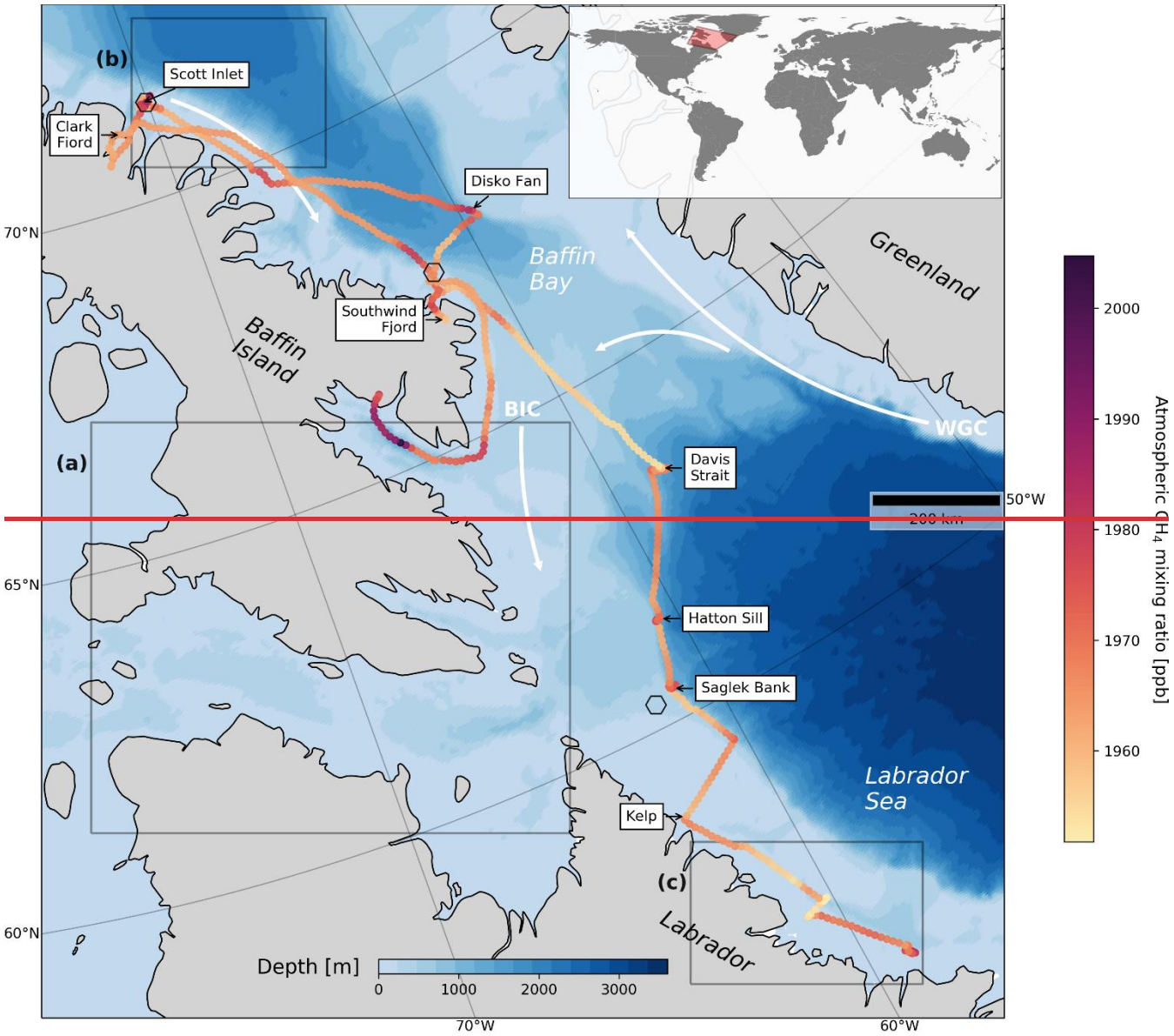

~~**Fig. 1: The ship's trajectory and atmospheric CH_4 levels as averages over consecutive 10 km sections. The black arrows point to the locations where water measurements were taken. The three black hexagons indicate confirmed or suspected locations of gas seepage (Punshon et al., 2014, 2019; Cramm et al., 2021). White arrows represent the West Greenland Current (WGC) and Baffin Island Current (BIC). Water depth was retrieved from the NOAA server (Amante and Eakins, 2009). Areas labelled a, b and c indicate the extents for each panel in Fig. 7.**~~

2.2 Atmospheric measurements

Instruments were mounted on the Meteorological Tower at the bow of the ship: A 2D heated anemometer (Model 86004, RM Young, USA) at a height of 8.1 m above deck~~,~~ and about 14.1 m above sea level (considering a constant height of the deck), a temperature probe (Model 107B, Campbell Scientific, USA) 7.6 m above the deck, a 1 Hz GPS puck (GPS 18x LVC, Garmin,

USA), and an air inlet for gas sampling at 7.3 m (Appendix A, Fig. A1). Roughly 30 m long Synflex tubing connected the air inlet with the greenhouse gas analyzer (Ultraportable Greenhouse Gas Analyzer, Los Gatos Research, USA), making ~~real-time~~high-resolution monitoring of atmospheric carbon dioxide (CO_2), methane (CH_4) and water ~~vapor~~vapour (H_2O) mixing ratios possible. In this study, all CH_4 and CO_2 measurements reflect dry mixing ratios. The analyzer is equipped with a built-in pump drawing the air from the inlet on the tower to the analyzer stored securely inside a laboratory on deck. The greenhouse gas analyzer was calibrated in July 2021 before deployment on the ship with certified calibration gas (calibrated by the AmeriFlux QA/QC team at the Lawrence Berkeley National Laboratory, Berkeley, CA, USA at 385.18±0.01 ~~ppm~~ppmv CO_2, 1810.6±0.1 ~~ppb~~ppbv CH_4, and 4.08±1.58 ~~ppm~~ppmv H_2O), and benchmarked daily (except for the first two days due to logistical issues) with a certified standard gas mixture (from Praxair) of 450 ~~ppm~~ppmv CO_2 balanced with air containing 5000 ~~ppb~~ppbv CH_4, which was well within the analyzer's measurement range (200−20,000 ~~ppm~~ppmv for CO_2 and 100−100,000 ~~ppb~~ppbv for CH_4). Once the setup was mounted and leak proof, we recorded atmospheric measurements ~~over a distance of 5100 km~~ between July 20, 2021, and August 10, 2021, on a datalogger (CR1000, Campbell Scientific, USA) at a frequency of 1 Hz.

We ~~pre-~~processed ~~the obtained data by excluding inconclusive~~wind measurement timeseries to exclude occasional erroneous values of ~~position, wind~~ direction and speed~~. Resulting gaps~~ , and ~~missing values of mixing ratios were~~ linearly interpolated~~, corresponding to 19% of all sampled 1 Hz data for gas mixing ratios. By repeatedly breathing on the air inlet, we determined an average delay time of 90 seconds for the air samples to reach the analyzer and accounted for this delay time during pre-processing~~ across gaps before resampling onto the datalogger's timestamp. Wind parameters were corrected for lateral ship motion when the ship was not in transit or not headed forward, using speed, track and heading from the ship's own navigation system ~~(Amundsen Science Data Collection, 2021c).~~(Amundsen Science Data Collection, 2021a).

By repeatedly breathing on the air inlet, we determined an average delay time of 90 seconds for the air samples to reach the analyzer and accounted for this delay time during data processing. The gas analyzer did not significantly drift over time (in comparison to the manufacturer's precision specification of 2 ~~ppb~~ppbv for 1 σ), and we assessed instrument noise and drift in combination by integrating the data from benchmarking while on the ship and determined a standard error of 2~~.1 ppb~~ ppbv for CH_4 and 0.13 ~~ppm~~ppmv for CO_2 that can be considered the uncertainty of our measurements. ~~In addition~~To exclude data potentially contaminated by the ship's exhaust, we ~~determined there~~excluded all measurements of CH_4 and CO_2, whenever the wind direction was ~~no significant~~80°−280° relative to the bow of the ship, and when CO_2 levels were larger than 420 ppm. As a result, 26 % of all 1 Hz CH_4 and CO_2 measurements were excluded on the account of potential contamination ~~of air samples by considering CO_2 mixing ratios when the air inlet was downwind of the ship's (comparatively elevated) exhaust.~~(see also Fig. A2). To determine CH_4 baseline levels for the studied region, we applied a Savitzky-Golay filter ~~(Savitzky and Golay, 1964)~~(Savitzky and Golay, 1964) of second polynomial order with a 24-hour window size on the mixing ratios.

Maxima in atmospheric CH_4 measurements were further investigated using the online Real-time Environmental Applications and Display System (READY) for the Hybrid Single-Particle Lagrangian Integrated Trajectory (HYSPLIT) model (Stein et al., 2015; Rolph et al., 2017). Ensemble back-trajectories of air masses from the time and location where CH_4 maxima were

measured (referred to as source) to the point of possible origin within the previous 12 hours were modelled. Two gridded meteorological data archives were used: the Global Data Assimilation System (GDAS) model (1° horizontal resolution) and the Global Forecast System (GFS) model (0.25° horizontal resolution). For the ensemble, the datapoints of the meteorological input model were offset by a fixed grid factor resulting in an output of 27 possible trajectories (Rolph et al., 2017).

Atmospheric pressure and dew point temperature measurements were recorded every two minutes with a digital barometer (PTB-210, Vaisala, Finland) and a humidity-temperature sensor (MP101A-T7, Rotronic, USA) located on the bridge of the ship ~~(Amundsen Science Data Collection, 2021b).~~(Amundsen Science Data Collection, 2021b). For statistical analyses, we ~~log transformed the non-normally distributed CH_4 mixing ratios,~~examined CH_4 measurements for linear Spearman rank correlations with available data and also fitted a simple Generalized Additive Model ~~(GAM; used previously in air quality studies, e.g. Pearce et al., 2011; Hou and Xu, 2022)~~(GAM; used previously in air quality studies, e.g. Pearce et al., 2011; Hou and Xu, 2022) to hourly averaged CH_4 data in order to identify trends of inter-dependencies. The GAM was well suited due to its ability to describe the non-linear effects of non-normally distributed data using non-parametric smoothing functions. The respective analysis was performed in R (package: "mgcv", function: "gam"; Wood, 2011).

2.3 Water column measurements

Seawater was collected at ~~13~~15 stations for measurements of dissolved CH_4: ~~north eastern~~Makkovik in the Labrador Shelf, northeastern Labrador ("Kelp"), two locations at Saglek Bank~~,~~ (Fig. A2), Hatton Sill, Davis Strait, Southwind Fjord, Disko Fan, ~~five~~six locations at Scott Inlet, and Clark Fiord (Fig. 1~~ and 2~~). While exclusively surface samples were taken at Clark Fjord and at four co-located stations close to the Scott Inlet seep (SI1, SE-1K, NE-1K, NE-5K; Fig. A2), we gathered water column profiles at the remaining ~~eight~~ten locations. Collection and measurement protocols followed that of Punshon et al. (2014, 2019). Briefly, seawater ~~from discrete depths was~~ samples were collected ~~into~~from 12 L Niskin bottles mounted on a Conductivity-Temperature-Depth (CTD~~))~~/Rosette~~. On recovery, the waters were transferred~~ system to 60 ml glass serum bottles (after triple rinsing with the sample water) to overfilling by 1.5 times the bottle volume, immediately fixed with mercuric chloride, capped with metal crimp seals and rubber septa, and stored at 4 °C. Samples were analyzed for CH_4 at the Bedford Institute of Oceanography (Department of Fisheries and Oceans, Canada) using a single-phase batch headspace equilibration method with gas chromatography (similar to Neill et al., 1997). ~~Uncertainty in dissolved CH_4 was ±0.08%~~Marine CH_4 concentrations are given in nmol/L, abbreviated as nM hereinafter. The analytical precision was estimated from repeat measurements of standard gases and amounted to 0.5−0.8 % or better for dissolved CH_4 similar to previous studies (Punshon et al., 2014, 2019). Data from previous studies conducted in 2011, 2012 and 2016 (Punshon et al., 2014, 2019) were included here to examine regional patterns and temporal variations of dissolved CH_4 concentrations in the Baffin Bay. Potential temperature (θ) and density of seawater at atmospheric pressure (σ_θ) were calculated based on water temperature, pressure and salinity measured on the ship (SBE ~~9plus~~911 CTD, Seabird Scientific, Canada) ~~(Amundsen Science Data Collection, 2021d)~~(Amundsen Science Data Collection, 2021c) using the package 'seawater' in Python (calculations based on Bryden, 1973; Fofonoff and Millard, 1983; Millero and Poisson, 1981). Water masses were ~~assigned according to operational~~

~~definitions considering specified ranges of calculated potential temperature and density of seawater~~defined following previous studies (Table 1 in Sherwood et al., 2021; Stramma et al., 2004; Fratantoni and Pickart, 2007; Azetsu-Scott et al., 2012). These water masses comprise Halocline Water ($\sigma_\theta \leq 27.30$ kg/m³, $\theta \leq 0$ °C), Baffin Bay Water ($27.50 < \sigma_\theta \leq 27.80$ kg/m³, $\theta \leq 2$ °C), Labrador Shelf Water ($\sigma_\theta \leq 27.40$ kg/m³, $\theta \leq 2$ °C), Irminger Water ($27.30 < \sigma_\theta \leq 27.68$ kg/m³, $\theta > 2$ °C), Labrador Sea Water ($27.68 < \sigma_\theta \leq 27.80$ kg/m³, $\theta > 2$ °C), and to a lesser extent North East Atlantic ~~Sea~~Deep Water ($27.80 < \sigma_\theta \leq 27.88$ kg/m³) and Denmark Strait Overflow Water (σ_θ ~~<~~> 27.88 kg/m³). It should be noted that surface waters (~2 m) did not necessarily match operational definitions of water masses as outlined in Sherwood et al. (2021) and were interpreted separately. We also used seawater density and oxygen data from the CTD casts (Amundsen Science Data Collection, 2021c) and determined the mixed layer depth where the density change was higher than 0.125 kg/m³ compared to the density at 5 m depth. Continuous water temperature and salinity measurements in surface waters from the underway thermosalinograph (Amundsen Science Data Collection, 2021d) were used to determine correlations with atmospheric measurements. Daily sea ice concentration data with 10 km resolution (AMSR-2, identifier OSI-408) by the Norwegian and Danish Meteorological Institutes was extracted from the Ocean and Sea Ice Satellite Application Facility EUMETSAT catalogue (https://thredds.met.no/thredds/osisaf/osisaf_seaiceconc.html; accessed: 2022-11-13).

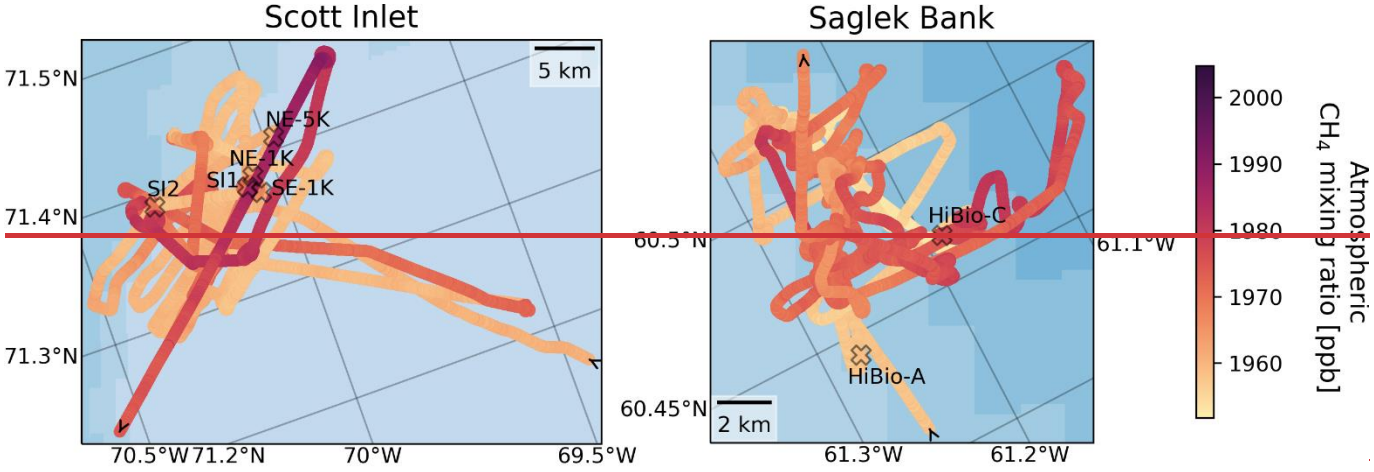

~~**Fig. 2: Close up of Scott Inlet and Saglek Bank, where multiple water measurements were taken. The locations of CTD Rosette sampling are indicated together with respective names of stations. The arrows indicate the direction where the ship was heading. Station SI1 was located at the seep at Scott Inlet (left panel).**~~

2.4 Sea-air methane flux

The instantaneous sea-air CH_4 flux (F) was determined with the bulk flux equation (Wanninkhof, 2014),

$$F = k\,(C_w - C_a),$$

combining measured dissolved CH_4 concentrations (C_w) and air-equilibrated seawater CH_4 concentrations (C_a) (Equation 7, Wiesenburg and Guinasso, 1979) ~~calculated with our atmospheric CH_4 measurements averaged between three minutes before and after the time of sampling, as well as water temperature and salinity measurements from the CTD. The gas transfer velocity (k) (Wanninkhof, 2014) was determined~~ calculated with our atmospheric CH_4 measurements averaged between five minutes

before and after the time of sampling, as well as water temperature and salinity measurements from the CTD (Amundsen Science Data Collection, 2021c). The gas transfer velocity (k) was determined after Ho et al. (2006) with

$$k = 0.251\,\bar{U}^2 254\,\overline{u_{10}}^2\,(Sc/660)^{-0.5},$$

making use of the Schmidt number (Sc) (Table 1, Wanninkhof, 2014) and wind speeds averaged between three minutes before and after the time of sampling ($\bar{U}$).

making use of the Schmidt number (Sc) with a correction for salinity (average 4.9 % diffusivity decrease for dihydrogen and helium in a seawater-like solution) based on Jähne et al. (1987), following the example of Manning et al. (2022) and the respective code (Manning and Nicholson, 2022) was used as a reference (see Appendix A2). Wind speeds were corrected to 10 m height via wind profile power law (Hsu et al., 1994) and averaged between five minutes before and after the time of sampling ($\overline{u_{10}}$). Positive sea-air fluxes indicated CH_4 flux from the ocean to the atmosphere. No flux was calculated for the Makkovik station since these samples were taken before atmospheric measurements had started.

3 Results and discussion

Seawater samples showed wide ranges of dissolved CH_4 concentrations at the different sample locations and water depths from undersaturated (5325 %, 0.29 nM) to highly oversaturated (6858%, 272.411324 %, 445.3 nM, Fig. 32). The by far highest water column concentrations were measured about 8 km north-west ofat the known cold seep at Scott Inlet (station SI2Stn0, Fig. 2) at 200A3) close to the bottom of the ocean (about 250 m water depth,), decreasing to 1213% (41.8133 % (3.6 nM) at the surface. TheseThe high concentrations close to the seafloor were not surprising given documented ebullition observed previously in the area (Cramm et al., 2021). The second depth profile taken in proximity to the seep, about 8 km northeast of its location (station SI2, Fig. A3) showed a maximum of 25.4 nM (639 %, Fig. 2) at 200 m depth and just slightly oversaturated surface water (113 %, 3.9 nM). Measurements from the year 2012 revealed CH_4 maxima of 65.8 nM at 200 m depth decreasing to 3.7 nM at the surface roughly 40 km north-westnorthwest from the seep location (Punshon et al., 2019). Large temporal fluctuations of dissolved CH_4 levels between 9 and 609 nM within 24 hours were found close to the seafloor (~250 m) at the seep in 2018 (Cramm et al., 2021). Similarly, other studies also manifested the temporal variability of seafloor seep degassing (Boles et al., 2001; Leifer and Boles, 2005; Shakhova et al., 2014; Cramm et al., 2021; Dølven et al., 2022)(Boles et al., 2001; Leifer and Boles, 2005; Shakhova et al., 2014; Cramm et al., 2021; Dølven et al., 2022). However, concentrationsConcentrations at the water surface of the seep were in the single digits in the pastpreviously (Cramm et al., 2021). Where high bottom concentrations within 5 km of the seep were measured, which was confirmed in Cramm et al. (2021), we found elevated concentrations between 42.7 nM (this study (from 3.9 nM at station NE−5K, roughly 5 km north-east of the seep) and 56.9 nM (SI2 to 5.3 nM at station SE−1K, about 1 km south-east of the seep) at the water surface (Fig. 2 and 3). Considering the findings from Punshon et al. (2019), Cramm et al. (2021)), and the present study, depths of ~200−250 m around the Scott Inlet seep location seemed most prominent for CH_4 maxima. Furthermore, elevatedwater columns supersaturated with CH_4 concentrations atin proximity to this location over several years showsshow the persistence of the

seep activity. Surface concentrations ~~an order of magnitude higher in 2021~~close to the atmospheric equilibrium in 2012, 2018 and 2021 in this area may indicate ~~reduced~~significant oxidation of CH_4 within the upper water column ~~relative to other years. However, this station~~. The Scott Inlet stations should not be considered as representative of the Baffin Bay as a whole, but rather specific to the seep location.

Seawater oversaturated with CH_4 (338 %, 12.9 nM) was also found at 250 m depth at Makkovik (Fig. 2), the southernmost station in this study. The ~~second highest concentrations~~Makkovik station was characterized by a strong gradient of water masses, with warm (6.3 °C) surface water, cold (~0 °C) sub-surface water featuring its CH_4 maximum and again warmer (3.8 °C) water at the seafloor.

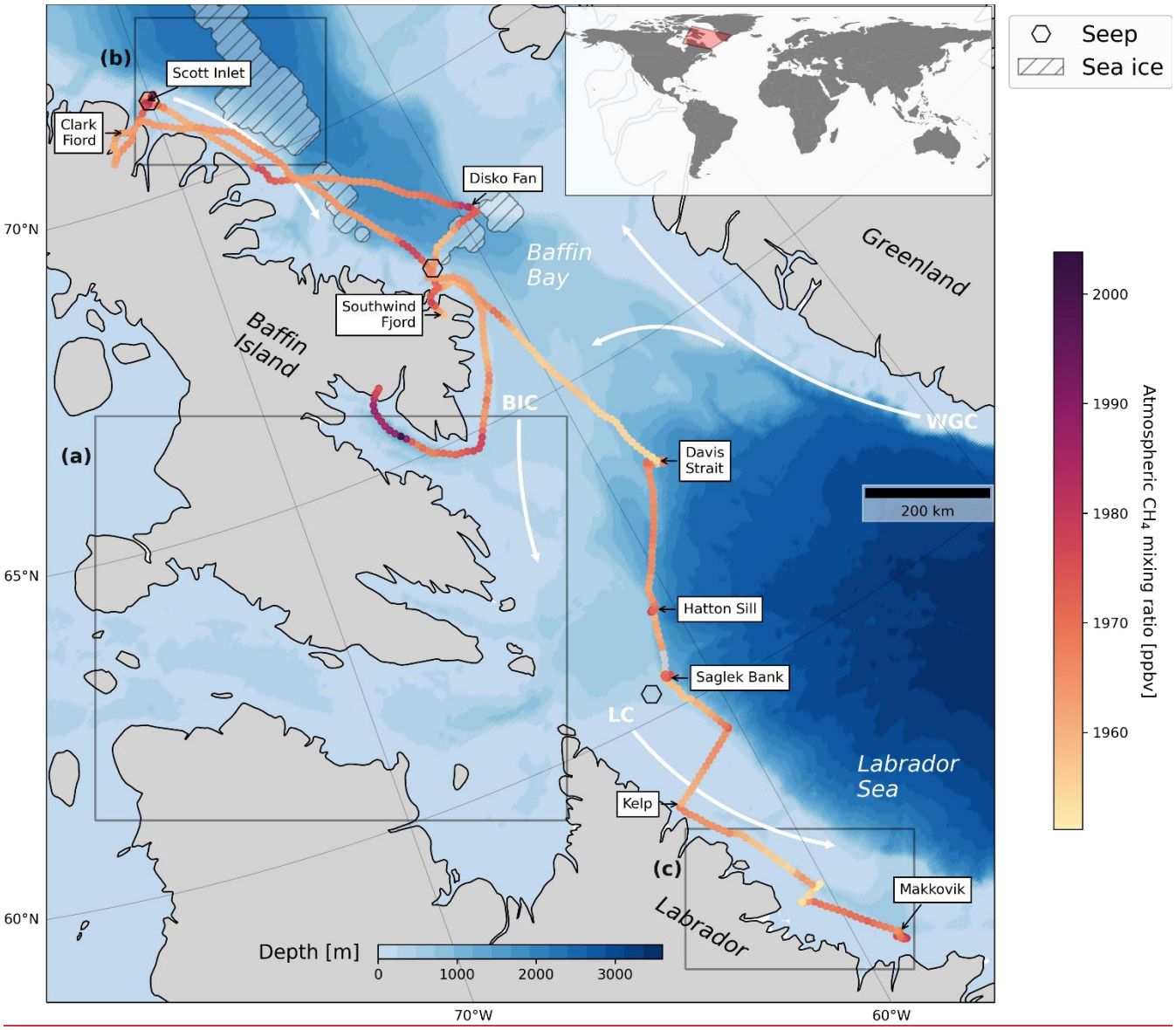

Fig. 1: The ship's trajectory and atmospheric CH_4 levels as averages over consecutive 10 km sections. The black arrows point to the locations where water measurements were taken. The three black hexagons indicate confirmed or suspected locations of gas seepage (Punshon et al., 2014, 2019; Cramm et al., 2021). White arrows represent the West Greenland Current (WGC), Baffin Island Current (BIC) and Labrador Current (LC). Water depth was retrieved from the NOAA server (Amante and Eakins, 2009). Areas labelled a, b and c indicate the extents for each panel in Fig. ~~dissolved CH_4~~A4. Shaded areas represent sea ice cover above 10 % (copyright 2021, EUMETSAT).

Dissolved CH_4 levels of similar range were measured at Southwind Fjord with a maximum of ~~2418~~227 % oversaturation (~~938~~.8 nM) at 30 m depth, ~~1578% (55.7~~148 % (5.2 nM) at the surface, and ~~1210% (48.0~~114 % (4.5 nM) at the bottom (75 m). Occurrences of highly supersaturated waters in Artic and sub-Arctic fjords have been documented previously: up to 33.5 nM and 974 % super-saturation in the Isfjorden, Svalbard, Norway (Damm et al., 2021), up to 72.3 nM and ~2000 % super-

saturation in the Storfjorden, Svalbard, Norway (Mau et al., 2013) and up to 459.2 nM at the head of the Canadian sub-Arctic Saguenay fjord (Li et al., 2021). ~~Possible sources of high dissolved CH_4 concentrations at Southwind Fjord in this study could be terrestrial runoff, although Manning et al.~~Most likely, the recent disturbance from iceberg groundings and subsequent landslides at Southwind Fjord (Normandeau et al., 2021) led to CH_4 release into the water column from a fresh supply of organic matter and lowered oxygen levels (Bonaglia et al., 2022). Other possible sources of enhanced dissolved CH_4 concentrations at this location could be terrestrial runoff (Castro-Morales et al., 2022), although Manning et al. (2022) found that rivers did not discharge significant amounts of CH_4 to the North American Arctic Ocean in the summers of 2017−2019. Advection of CH_4-rich water from other sources within the Baffin Bay could play an important role given the evidence of oil slicks off Cape Dyer for example (Budkewitsch et al., 2013). ~~Other potential sources could be unknown seeps within the fjord or the recent disturbance from iceberg groundings and subsequent landslides (Normandeau et al., 2021), which could have led to CH_4 release into the water column from a fresh supply of organic matter, or gas hydrates or CH_4 bearing pore water in the seafloor sediment disturbed by the turbulence~~Otherwise, gas hydrates or CH_4-bearing pore water in the seafloor sediment disturbed by the turbulence of local landslides (Paull et al., 2002)~~.~~ could have resulted in CH_4 release into the water column. Overall, we recommend follow-up sampling to assess the persistence of the CH_4 ~~super-saturation~~oversaturation and its source at Southwind Fjord.

CH_4 saturations at the remaining stations ranged between 25−178 % (0.9−6.9 nM) at varying depths. Compared to measurements at nearby locations in 2012 and 2016 (Punshon et al., 2014, 2019), dissolved CH_4 concentrations in 2021 at the stations Hatton Sill, HiBio-C, and Disko Fan were very similar ranging between 0.9−5.6 nM (Fig. 2). While concentrations at HiBio-A in all years showed similar ranges, a CH_4 peak of 6.8 nM (181 % saturation) in relatively shallow water at 50 m depth was observed in 2021 suggesting advection of CH_4 within subsurface water masses from elsewhere. Similar, relatively shallow CH_4-rich water masses brought along by the Labrador Current may have provoked the CH_4 maxima at Kelp and Makkovik. Methane concentrations in the general Davis Strait area measured one decade before (Punshon et al., 2014) were in good agreement with our findings for the respective station (1.8−5.4 nM).

In 2021, surface water concentrations were above saturation at all stations including further locations around the Scott Inlet seep and at Clark Fiord where only surface samples were taken (3.6−5.3 nM, 106−153 %, Fig. 3). Even though some sea ice was observed during the cruise, none of the water sample locations were in proximity to any significant sea ice cover (>10 %), so that local accumulation of CH_4-rich water below a surface ice layer as found previously (Damm et al., 2015) did not play a role here. A significant positive correlation of mixed layer mean dissolved CH_4 and oxygen levels at those stations where depth profiles were taken (Spearman $R^2 = 0.63$, $p < 0.01$) may suggest aerobic CH_4 production (Karl et al., 2008). Or else, sea ice melt may have discharged other precursors used by microbes to form CH_4 despite increasing oxygen levels towards the surface (Damm et al., 2015).

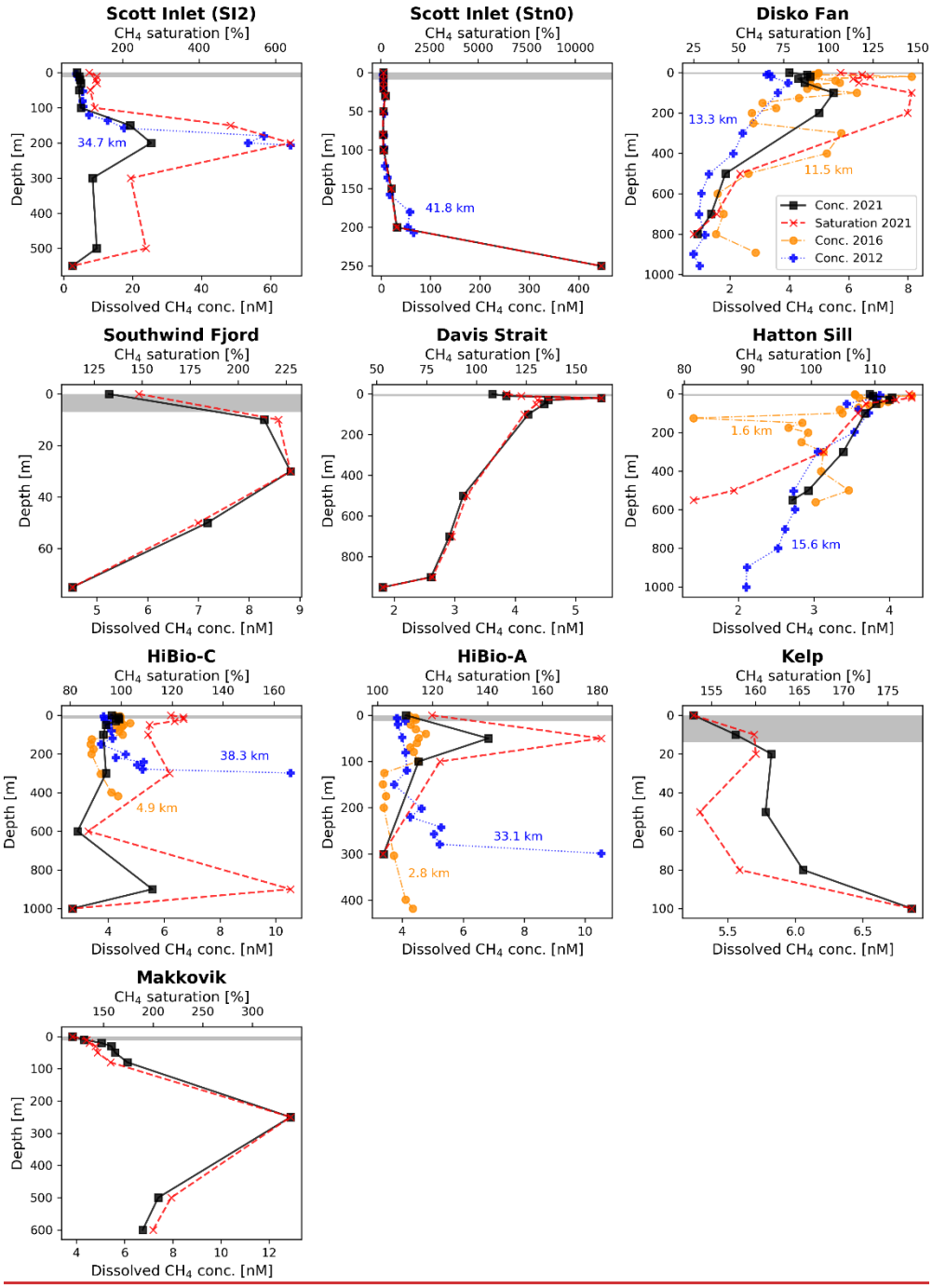

Fig. 2: Depth profiles of dissolved CH_4 concentrations (black) and saturations (red, dashed line) throughout the water column. Station names are given and can be located in Fig. 1 and A3. Profiles from Punshon et al. (2014, 2019) conducted in 2012 and 2016 were included for each year's closest stations within 50 km of the ones from 2021 and are shown in blue (2012) and orange (2016). Distances between respective nearby stations are given in kilometres. The mixed layer depths are indicated by gray areas.

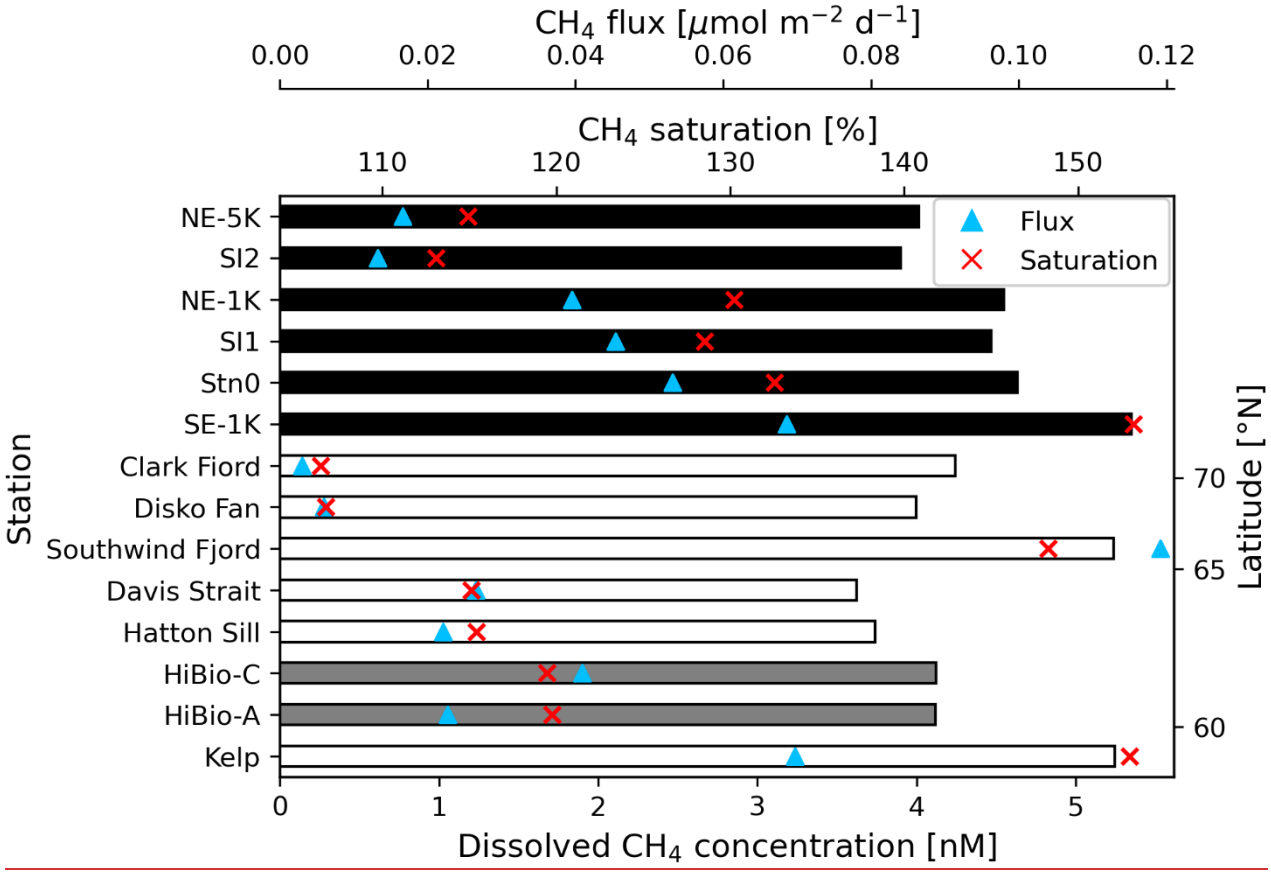

Fig. 3: Dissolved CH_4 concentrations at the water surface (bars) for all stations where CTD-Rosette samples and atmospheric measurements were collected. Gray bars represent two sample locations in the Saglek Bank area, and black bars reflect samples in the Scott Inlet area, both close to seafloor seep locations (station names correspond to those in Fig. A2). CH_4 saturations (red crosses) and estimated sea-air fluxes (blue triangles) are shown as well. Latitudes are not to scale.

The distribution of CH_4 with respect to water masses accounting for data from Punshon et al. (2014, 2019) and this study are visualized in a temperature-salinity diagram (Fig. 4). Samples span the known upper and intermediate depth of water masses of the

295 region, mainly Halocline Water (HW), followed by Irminger Water (

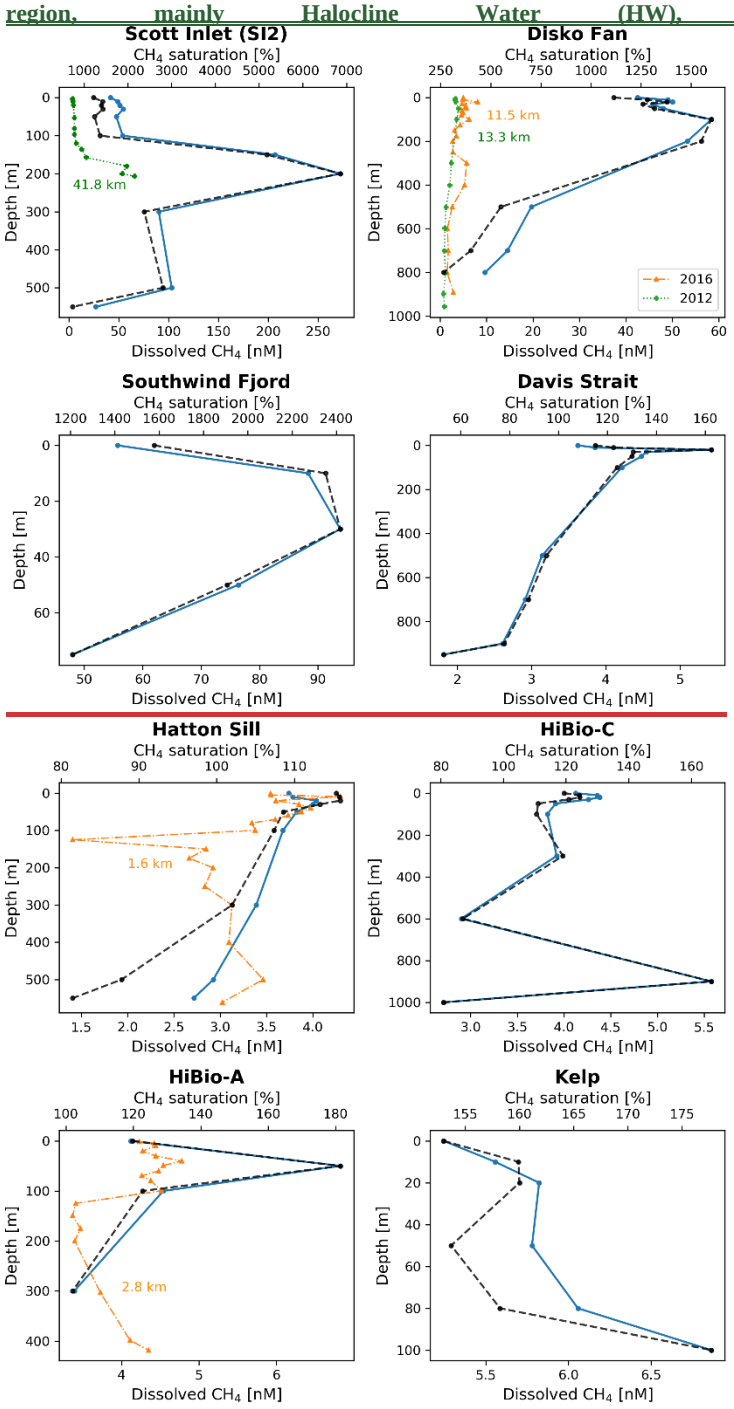

~~Fig. 3: Depth profiles of dissolved CH_4 concentrations (blue) and saturations (black, dashed line) throughout the water column. Station names are given and can be located on Fig. 1 and 2. Profiles from Punshon et al. (2014, 2019) conducted in 2012 and 2016 were included for stations close to the ones from 2021 and are shown in green (2012) and orange (2016). Distances between respective~~
300 ~~nearby stations are given in kilometres.~~

~~The Disko Fan station had concentrations of dissolved CH_4 that were the third highest in this study. The CH_4 maximum with a super-saturation of 1600% (58.4 nM) at 100 m depth, decreased with depth to 265% (9.7 nM) at 800 m, and remained high (>1000%) towards the surface. These results were much higher than measurements from nearby stations in 2012 and 2016 (Punshon et al., 2019) as shown in Fig. 3, and an order of magnitude higher than measurements on cross-basin transects (Punshon et al., 2014). While the cause of this increment remains unknown, prevailing currents (West Greenland Current) and the shallow depth of the CH_4 maximum (100 m) suggest a CH_4 source around the south-western Greenland shelf, where possible CH_4 seepage was suggested (Gregersen and Bidstrup, 2008; Gautier et al., 2011; Nielsen et al., 2014). Moreover, onshore lakes in south-west Greenland showed highest dissolved CH_4 concentrations (average of 2530 nM) among all reported lakes at northern latitudes (Northington and Saros, 2016), and glacial runoff from the Greenland ice sheet caused CH_4 discharge of an average 271 nM (Lamarche-Gagnon et al., 2019). Alternatively, increased CH_4 levels could originate from an extension of CH_4-rich water spreading from the western side of Baffin Bay. These findings also warrant the need of continued monitoring to see if high CH_4 levels at this location are persistent.~~

~~All other stations from Davis Strait and further southward along the northern Labrador shelf showed significantly lower dissolved CH_4 concentrations than any of the Baffin Bay stations. Respective subsurface maxima showed over saturation between 116–181% (4.0–6.9 nM) at varying depths. CH_4 concentrations at these stations except for "Kelp" tended to decrease with depth, suggesting advection of CH_4 within shallow water masses from elsewhere. Compared to measurements at nearby locations in 2016, dissolved CH_4 concentrations in 2021 at the stations Hatton Sill and HiBio-A were very similar ranging between 2.7–6.8 nM (Fig. 3). Average water column CH_4 concentrations of stations south of 65°N in 2021 (mean: 4.2 nM, range: 1.8–6.9 nM) were close to those measured in the Davis Strait in previous years (mean: 3.9 nM, range: 1.1–10.5 nM; Punshon et al., 2014, 2019).~~

~~The distribution of CH_4 with respect to water masses accounting for data from Punshon et al. (2014, 2019) and this study are visualized in a temperature-salinity diagram (Fig. 4). Samples span the known upper and intermediate depth of water masses of the region, mainly Halocline Water (HW), followed by Irminger Water (IM~~IW), Labrador Shelf Water (LShW) and Baffin Bay Water (BBW). Highest concentrations were found in Arctic HW (mean: ~~12~~10.3 nM, range: 2.4–~~272.44~~45.3 nM), which was ~~partly~~largely forced by the presence of the Scott Inlet seep (Fig. 4). This seep, and possibly others, could enrich the HW with CH_4 as HW travels southward in form of the Baffin Island Current. ~~HW overlying most of the water column at the Scott Inlet seep. This seep, and possibly others, could enrich the HW with CH_4 as HW travels southward in form of the Baffin Island Current.~~ The overall shallowest water mass, the LShW, held the second highest CH_4 concentrations (mean: ~~6.9~~4.3 nM, range: 1.1–~~88.3~~21.1 nM) partially due to direct seep impacts, and possibly ~~due to~~ the influence of the Baffin Island Current transporting CH_4-rich water southward or of the West Greenland Current carrying elevated CH_4 levels westward, which may have provoked ~~higher than expected~~elevated CH_4 ~~levels~~concentrations in LShW for example at Southwind Fjord, HiBio-A and possibly even at the ~~Disko Fan~~Makkovik station. Warmer IW masses ~~tended to have lower~~owned the third highest

concentrations (mean: 3.~~5~~2 nM, range: 1.~~3−53.2 nM), potentially due to increased~~0−10.5 nM). Increased oxygen availability was found in the Irminger Sea ~~as found in 2015 (Fröb et al., 2016) which could have led to CH_4 oxidation and reduced CH_4 levels, for example at the 2021 stations HiBio-A, HiBio-C, Hatton Sill and Davis Strait. Similarly, the~~in 2015 (Fröb et al., 2016), but dissolved oxygen levels during our Rosette casts showed lower oxygen concentrations on average in the IW than in the shallower HW and LShW. The colder and deeper BBW mass showed lower CH_4 concentrations (mean: ~~3.2~~1.7 nM, range: 0.2−~~103.2~~17.0 nM~~),~~) than the mostly oversaturated HW, LShW, and IW, whereas measurements in proximity to the Scott Inlet seep ~~and at the Disko Fan station in 2021~~ in 2021 and roughly 45 km north of the suggested seep at Cape Dyer in 2011 contributed to the high end (>~~17~~ 9 nM) of the concentration range~~. Therefore~~ for BBW. Most likely, both CH_4 production and consumption co-occurred in the BBW (Fenwick et al., 2017).

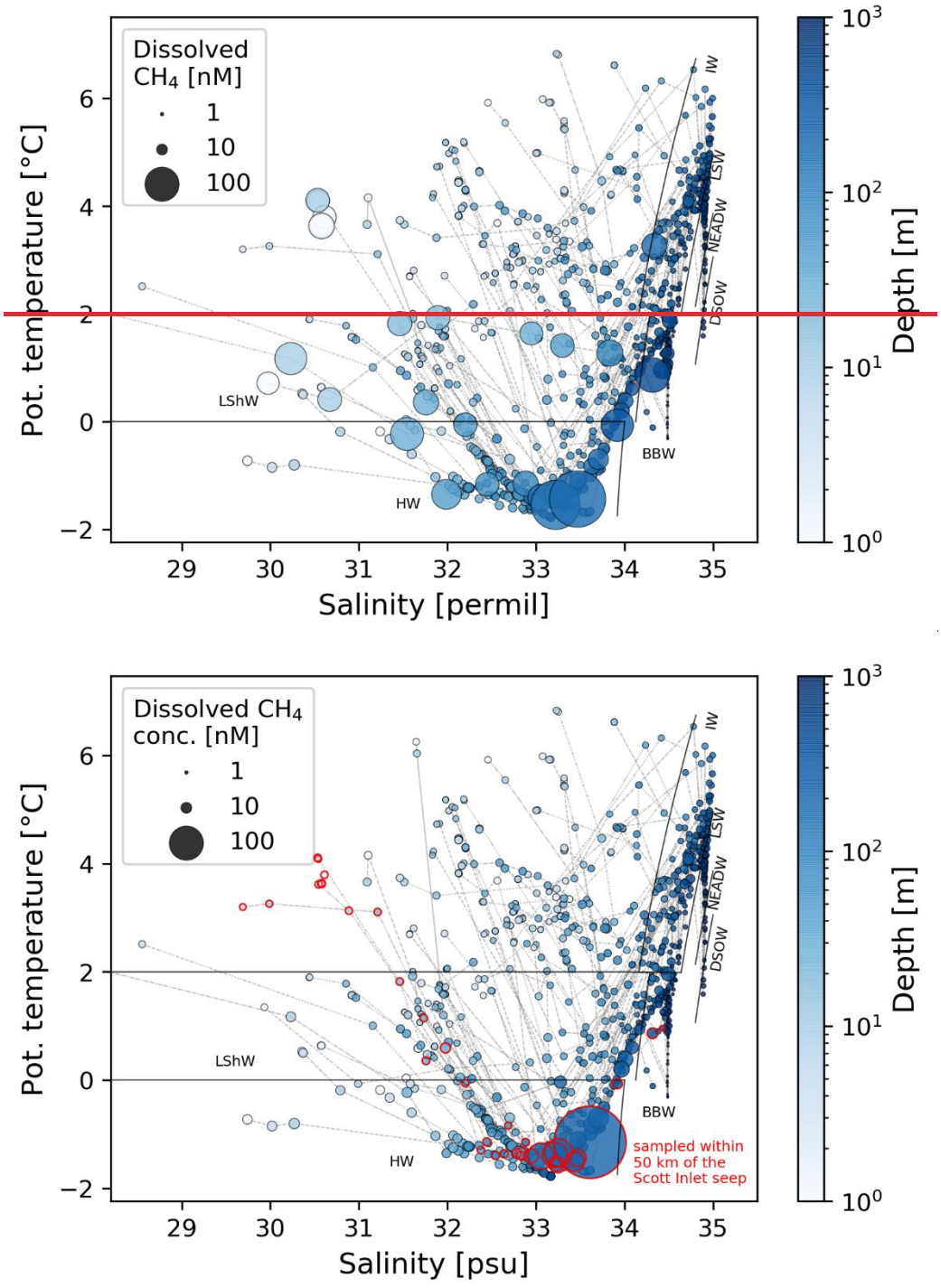

345

Fig. 4: Temperature-salinity diagram of all measurements from 2021 and from the studies by Punshon et al. (2014, 2019) for the Baffin Bay and Davis Strait area. Dissolved CH_4 concentrations are shown with different marker sizes, colors indicate the water depth. ~~Lines~~Black lines distinguish between water masses: Halocline Water (HW), Labrador Shelf Water (LShW), Irminger Water

(IW), Labrador Sea Water (LSW), Northeast Atlantic Deep Water (NEADW) and Denmark Strait Overflow Water (DSOW). Gray lines connect measurements from the same CTD-Rosette cast. For better visualization, salinities below 28‰ ~~which were~~ psu measured at the surface of the two fjords in 2021 are not shown. Red circles highlight the sample locations within 50 km of the seep in Scott Inlet.

~~In 2021, CH_4 concentrations decreased from subsurface maxima towards the surface at all stations (Fig. 3), which was most likely caused by oxidation within the water column. Nevertheless, surface water concentrations were above saturation at all stations (including further locations around the Scott Inlet seep and at Clark Fiord where only surface samples were taken, Fig. 5). While dissolved CH_4 concentrations at latitudes below 65°N ranged from 3.6–5.3 nM, concentrations were one order of magnitude higher in the sampled areas north of 65°N (41.8–56.9 nM). We suggest that differences in surface ocean current patterns with stronger influence of the West Greenland Current joining the Labrador Current (Tang et al., 2004; Curry et al., 2011) maintained lower concentrations of dissolved CH_4 at the water surface than above 65°N. Moreover, partial sea ice cover may also have reduced the diffusion of CH_4 from surface waters into the atmosphere in higher latitudes (Damm et al., 2015). We observed brief periods of close pack ice, but mostly brash ice between north of 65°N and south of Scott Inlet. High dissolved CH_4 concentrations at the surface of the (ice-free) Clark Fiord indicate that CH_4 rich water from waterbodies onshore could have been discharged into the narrow inlet (Manning et al., 2020; Li et al., 2021), or that other processes were responsible for the CH_4 accumulation.~~

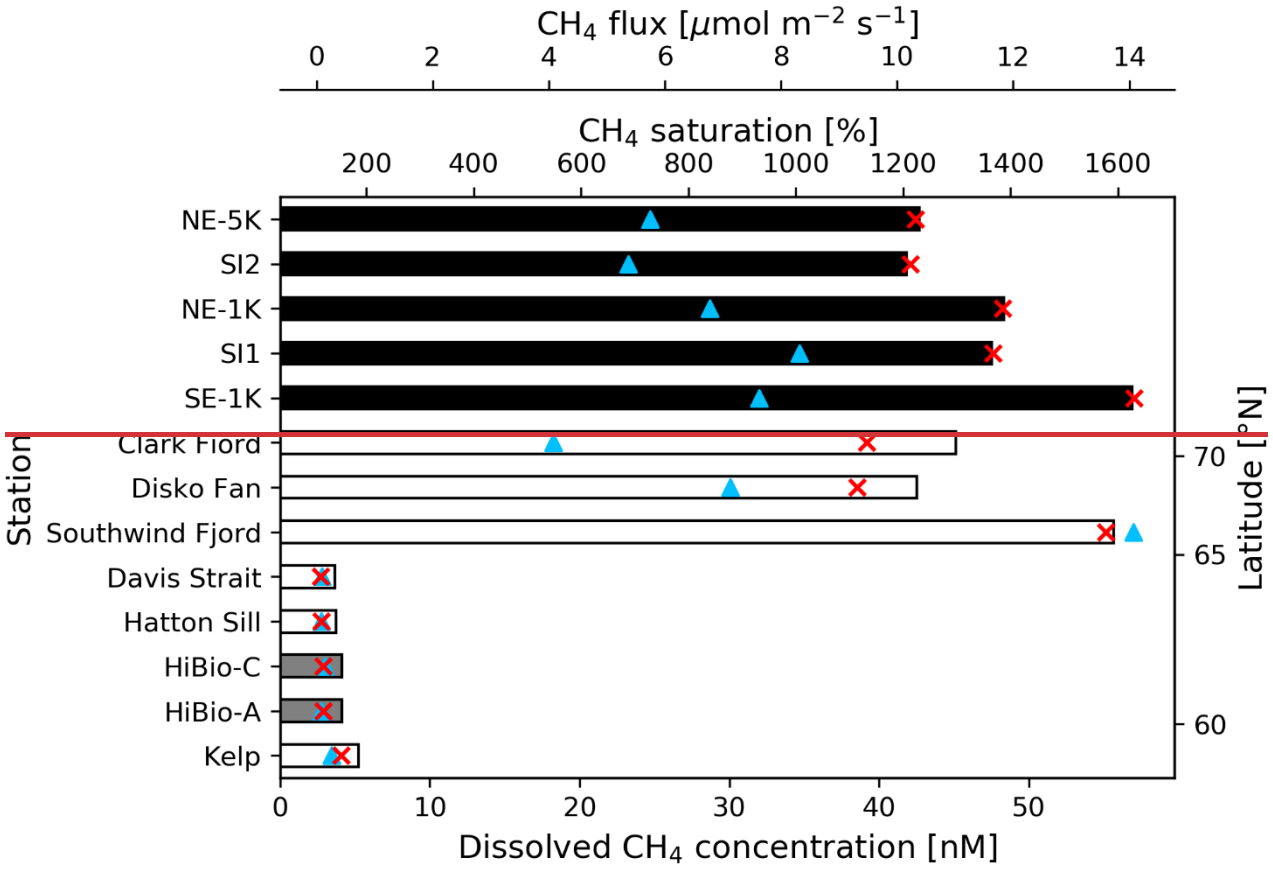

~~**Fig. 5: Dissolved CH_4 concentrations at the water surface (bars) for all stations where CTD-Rosette samples were collected. Gray bars represent two sample locations in the Saglek Bank area, and black bars reflect samples in the Scott Inlet area, both close to seafloor seep locations (station names correspond to those in Fig. 2). Concentrations north of 65°N were substantially higher than south of 65°N. CH_4 saturations (red crosses) and estimated sea-air fluxes (blue triangles) are shown as well. Latitudes are not to scale.**~~

~~In this study, we recorded a net flux of CH_4 from the ocean to the atmosphere, which amounted to a mean of 4.6±4.3 μmol m^{-2} d^{-1} based on measurements in 2021, with a mean of 0.1±0.1 μmol m^{-2} d^{-1} for measurement locations south of 65°N, and 7.4±3.0 μmol m^{-2} d^{-1} north of 65°N featuring large uncertainties. Overall, sea-air fluxes in this study peaked at 14.1 μmol m^{-2} d^{-1} in the Southwind Fjord, exceeding the flux rate of 5.4–8.3 μmol m^{-2} d^{-1} generated from the Scott Inlet seep (Fig. 5). As a result, fluxes in the northern Labrador Sea were negligible in summer 2021, whereas mean emission rates in the Baffin Bay beyond 65°N were of similar magnitude as mean estimates of 8.7 μmol m^{-2} d^{-1} for the Chukchi Sea (Thornton et al., 2020), and exceeded averages found in other studies of 1.6 μmol m^{-2} d^{-1} for the Davis Strait (Punshon et al., 2014), 1.3 μmol m^{-2} d^{-1} for the Bering Sea to Baffin Bay (Fenwick et al., 2017), and 0.4 μmol m^{-2} d^{-1} for the Baffin Bay and Davis Strait (Manning et al., 2022). Considering all measurements from 2021 and an area of 1,123,000 km^2 for the Baffin Bay and Davis Strait (Manning et al., 2022), we calculated a basin-wide mean net CH_4 flux of 0.030±0.029 Tg/yr (median: 0.035 Tg/yr, 25th percentile: 0.001 Tg/yr, 75th percentile: 0.047 Tg/yr). If samples with high concentrations were excluded, the net flux decreases to 0.021±0.036~~

~~Tg/yr (median: 0.001 Tg/yr, 25th percentile: 0.001 Tg/yr, 75th percentile: 0.024 Tg/yr), in which case the ocean may act as a small CH_4 source or sink to the atmosphere. Both flux estimates are one order of magnitude higher than the mean of 0.002±0.003 Tg/yr estimated for the Baffin Bay and Davis Strait by Manning et al. (2022). Therefore, the Baffin Bay and Davis Strait alone contributed on average 0.3% to the global oceanic CH_4 emissions of 9 Tg/yr (Saunois et al., 2020) based on our measurements in 2021.~~

Atmospheric CH_4 mixing ratios during the expedition ranged between 1944~~.7 ppb~~ ppbv off the coast of northern Labrador and 2012~~.0 ppb~~ ppbv in the Cumberland Sound in Nunavut (Fig. 1), with an overall mean (± standard deviation) of 1966~~.0±7.4 ppb.~~±8 ppbv. Wind speeds did not exceed 15 m/s. After ~~filtering~~applying the Savitzky-Golay filter to the measured data, baseline mixing ratios ranged between 1954~~.2 ppb~~ ppbv and ~~1980.6 ppb~~1981 ppbv (Fig. ~~6~~5). These concentrations were higher than global monthly mean CH_4 mixing ratios in July (1886~~.4 ppb~~ ppbv) and August (1892~~.6 ppb~~ ppbv) of the sampling year 2021 (Dlugokencky, 2022), but were within range of ~~recent (year 2020)~~ values from surface flask-air measurements from the year 2020 from northern stations of the NOAA Global Greenhouse Gas Reference Network, e.g. Summit, Greenland (July: 1939~~.2 ppb; August: 1946.7 ppb); Alert, Nunavut (July: 1933.0 ppb; August: 1945.7 ppb); Stórhöfði, Vestmannaeyjar, Iceland (July: 1937.9 ppb; August: 1952.8 ppb); and Ny Ålesund, Svalbard, Norway (July: 1955.2 ppb; August: 1962.4 ppb~~ ppbv; August: 1947 ppbv) and Alert, Nunavut (July: 1933 ppbv; August: 1946 ppbv) (Dlugokencky et al., 2021). The mixing ratios measured in this study are higher than those determined from flask samples likely due to the influence of CH_4 seeps in our study area. Our measured CH_4 values were ~~also~~ consistent with the known latitudinal gradient and recent ~~growth~~increase in atmospheric CH_4 (Lan et al., 2021). The baseline estimates suggest a local background CH_4 fluctuation of roughly ~~26 ppb~~27 ppbv in the studied area. A recent study found a contribution of 42.5±25.2 ~~ppb~~ppbv to total CH_4 mixing ratios measured during a cruise in the eastern Arctic Ocean, suggesting that atmospheric CH_4 levels over the ocean can be affected by distant wetland CH_4 sources (Berchet et al., 2020).

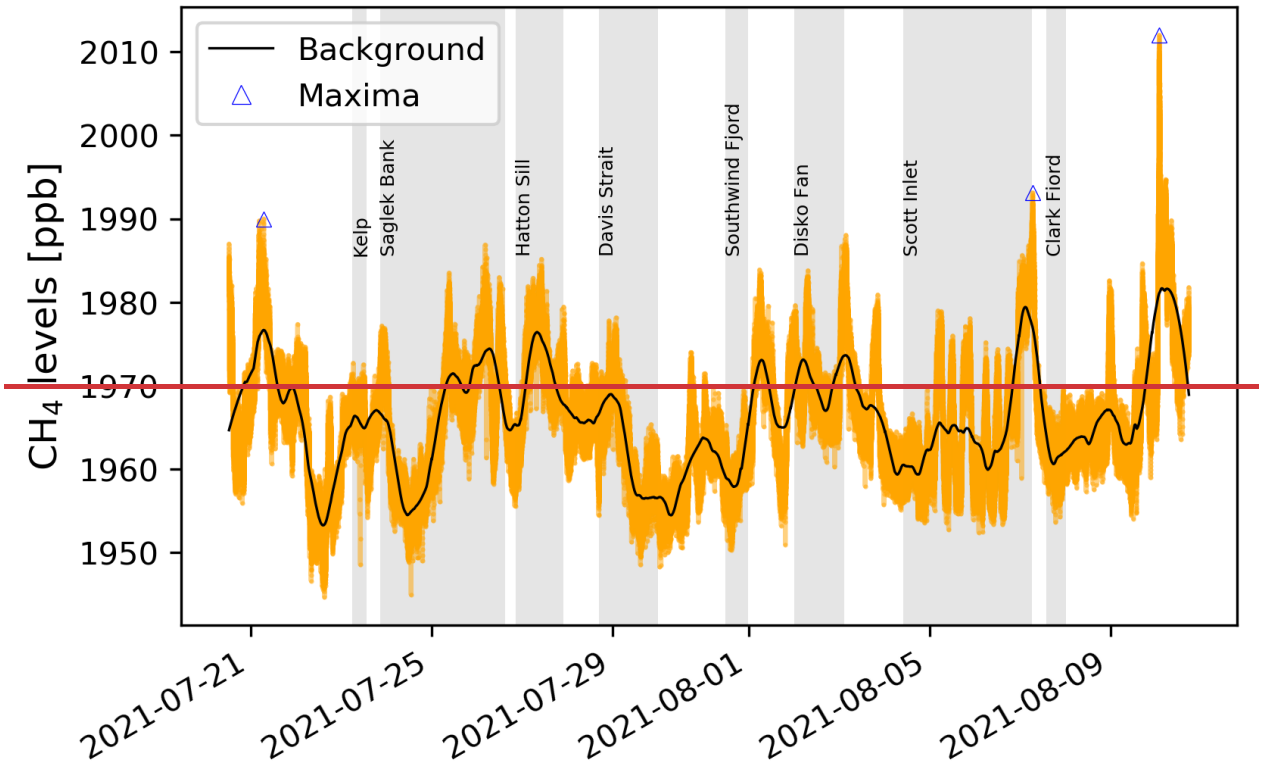
Background
Maxima
CH_4 levels [ppb]
2010
2000
1990
1980
1970
1960
1950
Kelp
Saglek Bank
Hatton Sill
Davis Strait
Southwind Fjord
Disko Fan
Scott Inlet
Clark Fiord
2021-07-21
2021-07-25
2021-07-29
2021-08-01
2021-08-05
2021-08-09

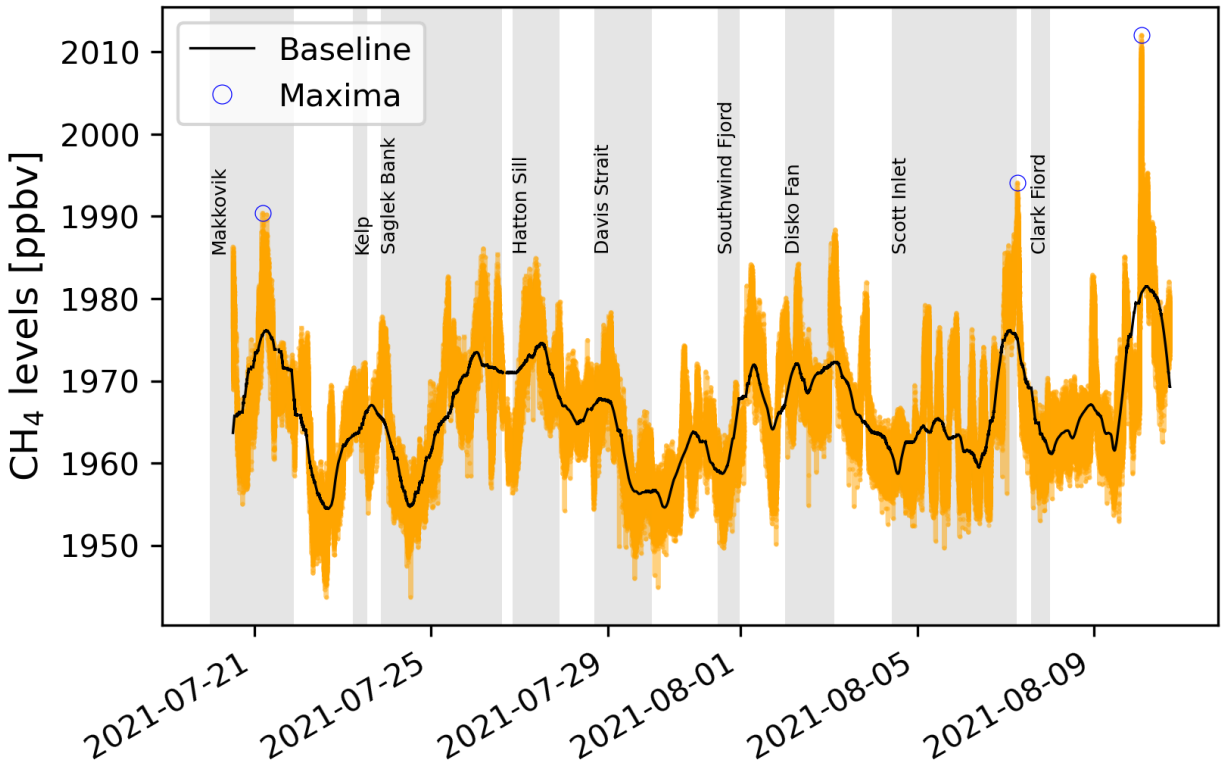

Fig. ~~6~~5: Timeseries of atmospheric CH_4 levels (orange points) and the derived ~~background levels~~baseline (black line) over the entire measurement period. Gray parts show the approximate duration at the stations ~~(Amundsen Science Data Collection, 2021a)~~(Amundsen Science Data Collection, 2021e), where seawater samples were collected. Blue ~~triangles~~circles reflect the three maxima of atmospheric CH_4.

~~Persistent enhancements of CH_4 mixing ratios above the baseline lasting over roughly 4 hours were detected repeatedly over the length of the expedition (Fig. 6). We investigated potential atmospheric origins of CH_4 maxima at three locations, Cumberland Sound, Scott Inlet, and the Labrador Trough, using ensemble back-trajectories (Fig. 7). At Cumberland Sound, the maximum of 2012.0 ppb coincided with prevailing westerly winds based on our measurements. Therefore, we assumed that those ensemble trajectories indicating air transport from or across the inland on the western side best reflected the observed meteorological conditions (Fig. 7a). Since no water samples were taken in the Cumberland Sound, where the highest atmospheric CH_4 levels were observed, we could not rule out an ocean-related atmospheric input of CH_4 at this location. Instead, we inferred from a back-trajectory analysis that the elevated CH_4 mixing ratios likely originated from sources onshore such as waterbodies or wetlands. The second highest CH_4 peak of 1993.1 ppb was detected roughly 12 km north-east of the Scott Inlet seep with dominating easterly winds (Fig. 2, left panel; Fig. 7b). Given the distance of roughly 500 km from Greenland, the origin of this CH_4 enhancement may rather be ocean based than land based, which suggests the existence of further seeps along the continental shelf east of Scott Inlet (Gregersen and Bidstrup, 2008; Gautier et al., 2011; Nielsen et al.,~~

~~2014). Trajectories for the third highest CH_4 levels of 1990.0 ppb measured in the Labrador Trough coupled with west-south-west wind directions suggested onshore sources from northern Labrador (Fig. 7c).~~

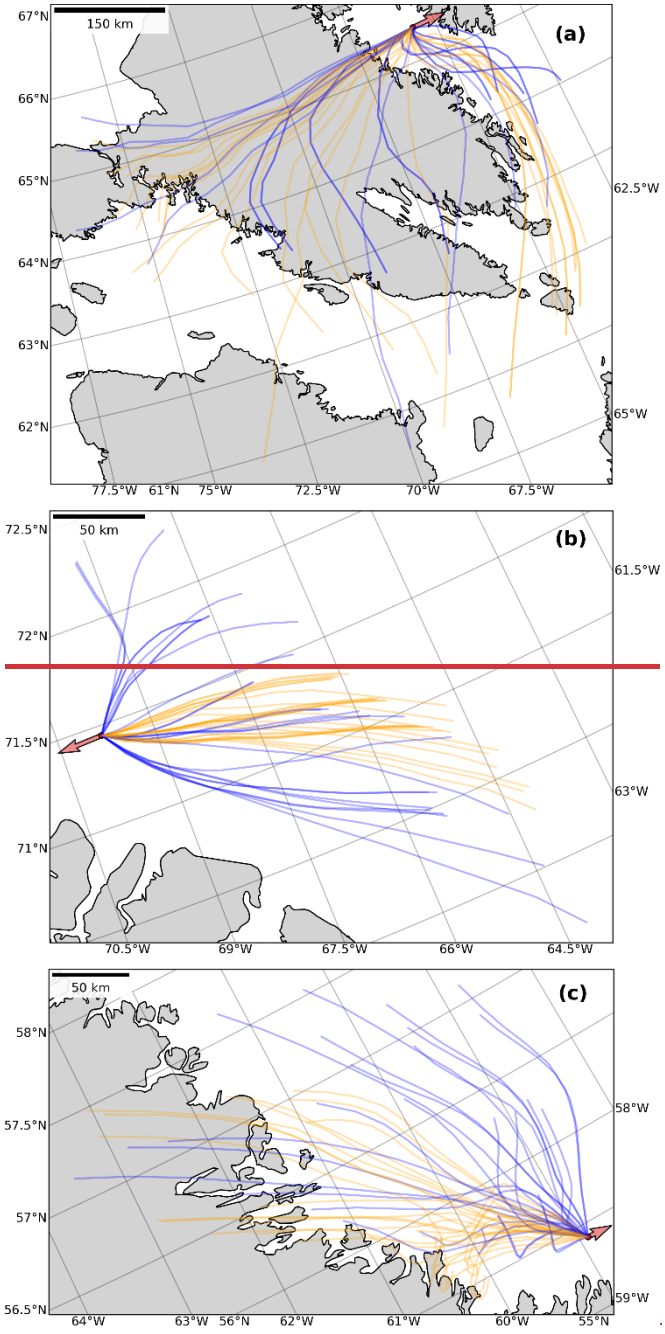

425 ~~**Fig. 7: Back trajectories of air masses approaching the locations where highest atmospheric CH_4 levels were measured in the Cumberland Sound (a), at Scott Inlet (b) and in the Labrador Sea (c). Orange lines represent trajectories using the GFS archive and blue lines show trajectories with the GDAS meteorological model.**~~ **Persistent enhancements of CH_4 mixing ratios above the baseline lasting over more than four hours were detected repeatedly over the length of the expedition (Fig. 5). We investigated potential**

atmospheric origins of CH_4 maxima at three locations, Cumberland Sound, Scott Inlet, and the Labrador Trough, using ensemble back-trajectories (Fig. A4). At Cumberland Sound, the maximum of 2012 ppbv coincided with prevailing westerly winds based on our measurements. Therefore, we assumed that those ensemble trajectories indicating air transport from or across the inland on the western side best reflected the observed meteorological conditions (Fig. A4a). Since no water samples were taken in the Cumberland Sound, where the highest atmospheric CH_4 levels were observed, we could not rule out an ocean-related atmospheric input of CH_4 at this location. ~~Red arrows indicate the direction of air movement averaged over three minutes before and after the time of sampling, pointing in the direction the wind is blowing to.~~

~~Calculated sea-air fluxes demonstrated that the ocean in the studied area acted as a CH_4 source to the atmosphere. However, linear correlations between atmospheric and dissolved CH_4 levels based on our dataset were not found which indicates that CH_4 released from seeps at the seafloor alone did not directly increase atmospheric CH_4 mixing ratios consistent with findings from previous studies (Law et al., 2010; Punshon et al., 2019; Cramm et al., 2021). Furthermore, linear correlations of CH_4 mixing ratios with available data were not found, suggesting more complex relationships at sea. Instead, results of a Generalized Additive Model proposed spatial (latitude, longitude), temporal (hour of day) and meteorological (pressure, dew point temperature) influences on atmospheric CH_4 mixing ratios with a good fit ($n=173$, $R^2=0.84$, 88% explained deviance). In this study, small increments of atmospheric CH_4 levels in proximity to seep locations were observed, whereas at other locations where substantial fluxes of CH_4 from the sea to the atmosphere were determined locally atmospheric concentrations were not noticeably affected. Therefore, we suggest that atmospheric CH_4 levels were influenced by a number of processes including, but not limited to seafloor seeps, upwind distant land based sources like wetlands and other waterbodies, weather conditions and ultimately temporal and spatial differences.~~

Instead, the back-trajectory analysis suggests that the elevated CH_4 mixing ratios could have originated from along the trajectories leading onshore, where potential sources such as waterbodies or wetlands could be located (Fisher et al., 2011; Thonat et al., 2017; Berchet et al., 2020). The second highest CH_4 peak of 1994 ppbv was detected roughly 13 km northeast of the Scott Inlet seep with dominating easterly winds (Fig. A4b). Given the distance of roughly 500 km from Greenland, the origin of this CH_4 enhancement could be ocean-based, with origins from further seeps along the continental shelf east of Scott Inlet (Gregersen and Bidstrup, 2008; Gautier et al., 2011; Nielsen et al., 2014). Trajectories for the third highest CH_4 levels of 1990 ppbv measured in the Labrador Trough coupled with west-south-west wind directions may suggest onshore sources from northern Labrador (Fig. A4c).

Linear correlations between atmospheric and dissolved CH_4 levels based on our dataset were not found. Due to the atmosphere-sea surface barrier, and complexities added by wind conditions, ocean currents, bacterial activity within the water column and other processes, the atmosphere-ocean system essentially describes a decoupled system locally, so that increased CH_4 concentrations are not necessarily found alongside rising atmospheric CH_4 levels (Law et al., 2010; Punshon et al., 2019; Cramm et al., 2021; Zhao et al., 2022). Accordingly, simple linear correlations of CH_4 mixing ratios with available auxiliary data (latitude, longitude, speed, wind speed and direction, air temperature, humidity, dew point temperature, atmospheric pressure, water temperature, salinity, hour of day) were not found, suggesting more complex relationships. Instead, results of a Generalized Additive Model proposed spatial (latitude, longitude), temporal (hour of day) and meteorological (atmospheric

pressure, dew point temperature) influences on hourly averaged atmospheric CH_4 mixing ratios with a good fit (n = 171, R^2 = 0.84, 88 % explained deviance) for the parts of the cruise when these data were available. Therefore, we suggest that atmospheric CH_4 levels were influenced by a number of processes including, but not limited to seafloor seeps, upwind distant land-based sources like wetlands and other waterbodies, weather conditions and ultimately temporal and spatial differences.

Based on our measurements, we determined a near-zero net flux of CH_4 from the ocean to the atmosphere, which amounted to a mean of 0.039±0.031 µmol m^{-2} d^{-1} along Baffin Island and Labrador in 2021, compared to 1.6 µmol m^{-2} d^{-1} in Davis Strait in 2011 (Punshon et al., 2014). Overall, sea-air fluxes in this study peaked at 0.119 µmol m^{-2} d^{-1} in the Southwind Fjord, exceeding the flux rates at the Scott Inlet seep (Fig. 5). As a result, fluxes in the northern Labrador Sea and Baffin Bay were negligible in summer 2021 in comparison to mean estimates of 8.7 µmol m^{-2} d^{-1} for the Chukchi Sea (Thornton et al., 2020), of 1.3 µmol m^{-2} d^{-1} for the Bering Sea to Baffin Bay (Fenwick et al., 2017), or of 0.4 µmol m^{-2} d^{-1} for the Baffin Bay and Davis Strait from measurements between 2015−2019 (Manning et al., 2022).

4 Conclusion

Continuous measurements of atmospheric CH_4 levels in ~~remote marine regions of~~ the northern Labrador Sea and Baffin Bay ~~made this study unique~~were above the global marine average with small instantaneous input from the ocean. Differences in dissolved CH_4 concentrations were mainly affected by ocean currents and seafloor sources, while atmospheric CH_4 levels showed interrelations with environmental conditions, location, and time with small temporal fluctuations. ~~Ocean~~Both ocean-based CH_4 sources as well as onshore waterbodies and wetlands likely contributed to atmospheric CH_4 levels. Further investigation is necessary to confirm potential CH_4 sources, for example through analyses of carbon isotopic ratios~~.~~ and more extensive back-trajectory modelling. We suggested baseline CH_4 mixing ratios between 1954~~.2 ppb~~ ppbv and ~~1980.6 ppb~~1981 ppbv for the studied area which can be used to validate global-scale measurements and modelling. Depth profiles and their comparison with measurements from previous years in the studied area revealed little interannual variation and ongoing CH_4 to the hydrosphere from the Scott Inlet cold seep. More extensive investigation of the chemical composition of sediments, bacterial activity, and riverine input could help explain elevated CH_4 levels within the shallow water column at Southwind Fjord, where recent landslides triggered by an iceberg were observed. Even though the Arctic Ocean does currently not contribute significantly to the global CH_4 budget as found by other studies, monitoring and investigation of CH_4 levels in and over the sea ~~remains~~remain relevant to assess potential impacts of climate change in regions susceptible to permafrost thaw, destabilization of CH_4 hydrates and reduced sea ice cover.

Appendix A

A.1 Figures

Fig. A1: The measurement tower at the bow of the ship with anemometer, temperature sensor, and air inlet mounted on the truss approximately where the arrow is pointing. The GPS was fixed at the lower end of the truss. Photo credit to David Cote (DFO, Canada).

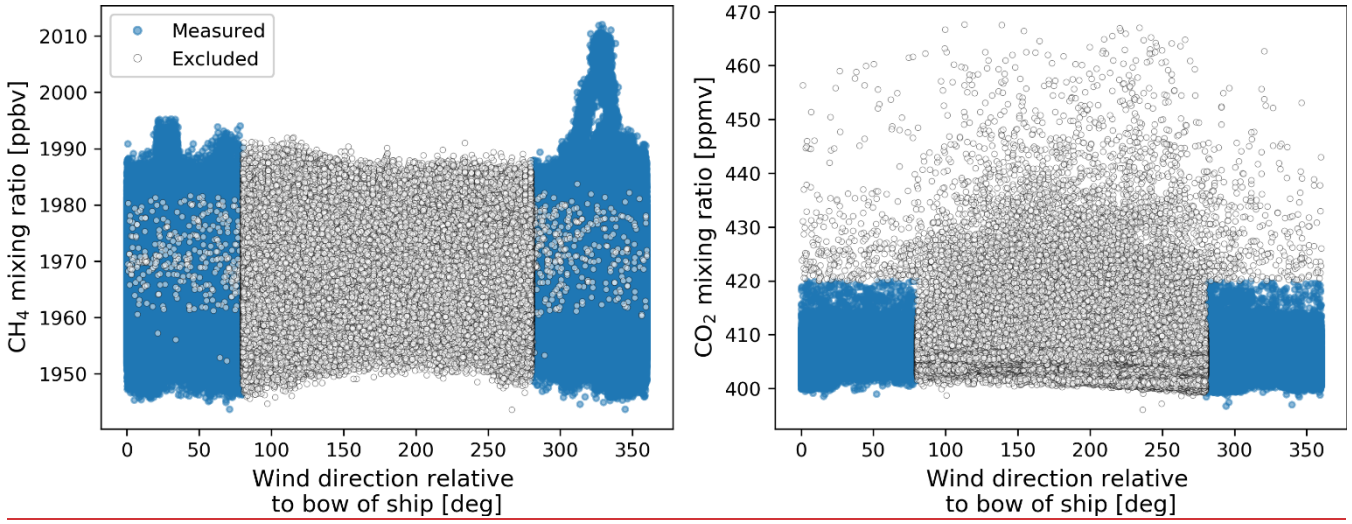

Fig. A2: Gas mixing ratios throughout the cruise for wind directions relative to the bow of the ship are shown. All data represented by open circles fulfil the criterion for measurements potentially contaminated by the ship's exhaust (wind directions between 80–280° or CO_2 mixing ratios < 420 ppm) amounting to 26 % of all measured 1 Hz data.

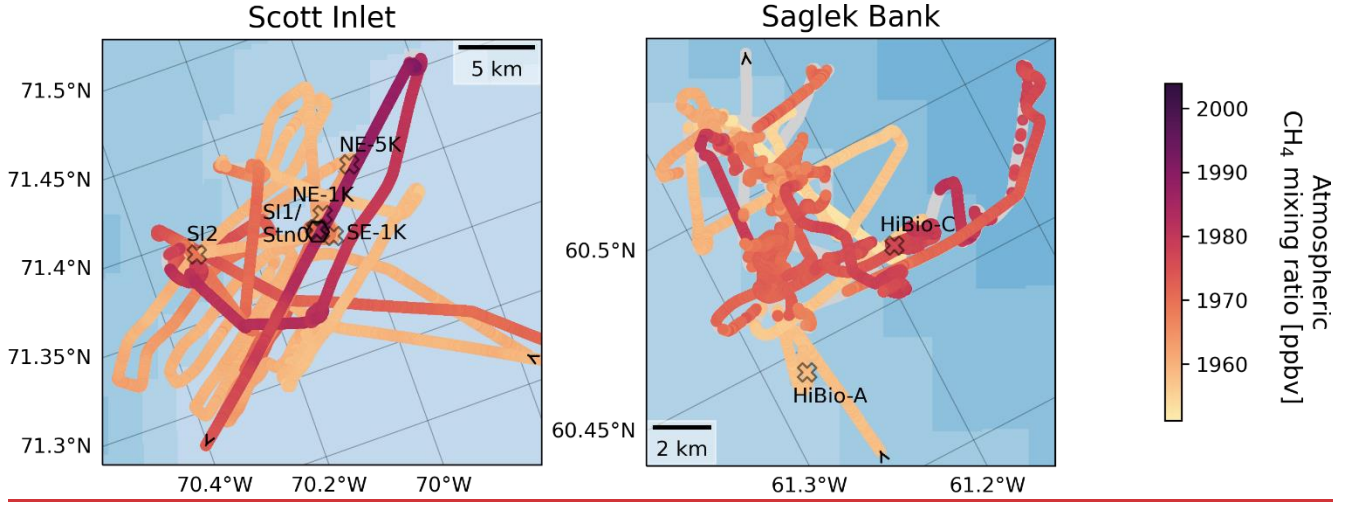

Fig. A3: Close-up of Scott Inlet and Saglek Bank, where multiple water measurements were taken. The locations of CTD-Rosette sampling are indicated together with the respective names of stations. The arrows indicate the direction where the ship was heading.

Stations SI1 and Stn0 were co-located at the Scott Inlet seep (black hexagon, left panel). Gray circles indicate measurements excluded due to the ship's contamination.

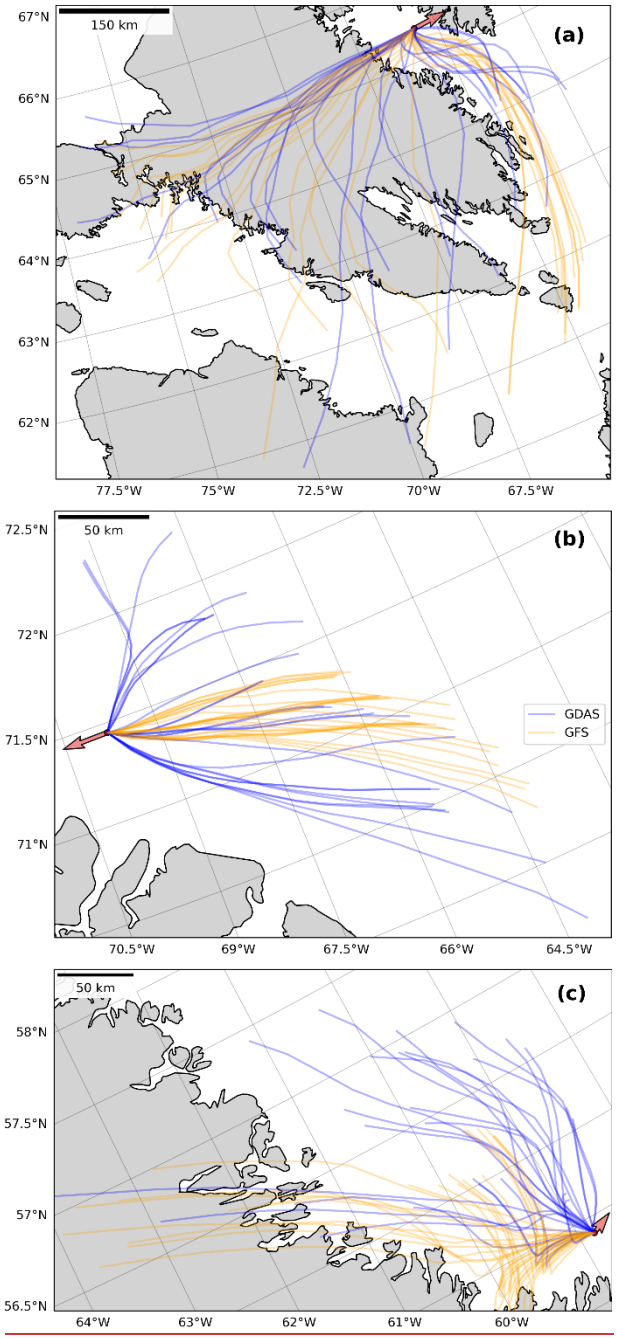

Fig. A4: Back-trajectories of air masses approaching the locations where highest atmospheric CH_4 levels were measured in the Cumberland Sound (a), at Scott Inlet (b) and in the Labrador Sea (c). Orange lines represent trajectories using the GFS archive and blue lines show trajectories with the GDAS meteorological model. Red arrows indicate the direction of air movement averaged over five minutes before and after the time of sampling, pointing in the direction the wind is blowing to.

A.2 Flux estimates

To determine the sea-air fluxes, the wind profile power law following Hsu et al. (1994) was used to correct wind speeds in m/s from the anemometer at 14.1 m height above sea level to 10 m height:

$$u_{10} = u_{14.1} \frac{10}{14.1}^{0.11}.$$

Furthermore, the Schmidt number for CH_4 in sea water following the example of Manning and Nicholson (2022) based on Jähne et al. (1987) was incorporated:

$$Sc = \frac{\mu_w}{D_w},$$

with the kinematic viscosity of seawater (Manning and Nicholson, 2022):

$$\mu_w = 0.0001 \cdot (17.91 - 0.5381 \cdot T_w + 0.00694 \cdot {T_w}^2 + 0.02305 \cdot S_w) \cdot \frac{1}{\rho_w},$$

the water temperature (T_w) in °C, salinity (S_w) in psu as measured by the CTD, and density at atmospheric pressure (ρ_w) in kg/m³ (Fofonoff and Millard, 1983; Millero and Poisson, 1981).

The diffusion coefficient (D_w) in m²/s was determined following Manning and Nicholson (2022) and based on Jähne et al. (1987):

$$D_w = 3.0470 \cdot 10^{-6} \cdot e^{\frac{-18360}{R \cdot (T_w + 273.15)}} \cdot (1 - 0.049 \cdot S_w / 35.5),$$

using the ideal gas constant $R = 8.314510 \frac{kg\ m^2}{s^2\ K\ mol}$.

Data availability

Data was made publicly available: Vogt, J., Risk, D., Azetsu-Scott, K., Edinger, E. N. & Sherwood, O. A.: Methane flux estimates from continuous atmospheric measurements and surface-water observations in the northern Labrador Sea and Baffin Bay, https://doi.org/10.5683/SP3/6IUECA, Borealis, V5, 2022.

Author contribution

JV, DR and OAS designed and conceptualized the study and JV collected the data. EB processed the raw atmospheric data. KAS provided the resources for seawater analysis and ENE mentored. JV prepared the manuscript with contributions from all co-authors.

Competing interest

The authors declare that they have no conflict of interest.

Acknowledgements

We would like to thank the teams from Amundsen Science and the Canadian Coast Guard for their incredible work in preparation of, and during leg 2 of the 2021 expedition. Some of the data presented herein were collected by the Canadian research icebreaker CCGS *Amundsen* and made available by the Amundsen Science program, which is supported through Université Laval by the Canada Foundation for Innovation. We also thank FluxLab members for their support during equipment ~~and data~~ preparation, especially ~~Dr. Evelise Bourlon,~~ Isaac Ketchum and Daniel Wesley. We thank Dr. Carrie-Ellen Gabriel and Darlene Childs for analyzing the seawater samples, and Dr. Simone Booker, Shaomin Chen and other cruise participants who assisted in the sample collection. Funding was provided by an NSERC ship time grant to Dr. Owen Sherwood and others (RGPST-544990-2020) and a NSERC Discovery Grant awarded to Dr. Owen Sherwood (RGPIN-2018-05590). Seawater analysis was funded through The Aquatic Climate Change Adaptation Services Program (ACCASP) of DFO.

References

Amante, C. and Eakins, B. W.: ETOPO1 1 Arc-Minute Global Relief Model: Procedures, Data Sources and Analysis, NOAA Tech. Memo. NESDIS NGDC, 24, 19, 2009.

Amundsen Science Data Collection: Amundsen Science field station lists, ~~Canadian~~Can. Cryospheric ~~Information Network (~~Inf. Netw. CCIN~~),~~ Waterloo~~, Canada, 2021a~~ Can., 2021e.

Amundsen Science Data Collection: AVOS Meteorological Data collected by the CCGS Amundsen in the Canadian Arctic, ~~Canadian~~Can. Cryospheric ~~Information Network (~~Inf. Netw. CCIN~~),~~ Waterloo~~, Canada~~ Can., Processed data, https://doi.org/10.5884/12518, 2021b.

Amundsen Science Data Collection: CCGS Amundsen Navigation (NAV) data recorded during the annual science expeditions in the Canadian Arctic., ~~Canadian~~Can. Cryospheric ~~Information Network (~~Inf. Netw. CCIN~~),~~ Waterloo~~, Canada, 2021c~~ Can., Complete data Version 1, https://doi.org/10.5884/12447, 2021a.

Amundsen Science Data Collection: CTD-Rosette data collected by the CCGS Amundsen in the Canadian Arctic, ~~Canadian~~Can. Cryospheric ~~Information Network (~~Inf. Netw. CCIN~~),~~ Waterloo~~, Canada~~ Can., Processed data Version 1, https://doi.org/10.5884/12713, 2021c.

Amundsen Science Data Collection: TSG data collected by the CCGS Amundsen in the Canadian Arctic, Can. Cryospheric Inf. Netw. CCIN Waterloo Can., Processed data Version 3, https://doi.org/10.5884/12715, 2021d.

Azetsu-Scott, K., Petrie, B., Yeats, P., and Lee, C.: Composition and fluxes of freshwater through Davis Strait using multiple chemical tracers, J. Geophys. Res. Oceans, 117, https://doi.org/10.1029/2012JC008172, 2012.

Berchet, A., Pison, I., Crill, P. M., Thornton, B., Bousquet, P., Thonat, T., Hocking, T., Thanwerdas, J., Paris, J.-D., and Saunois, M.: Using ship-borne observations of methane isotopic ratio in the Arctic Ocean to understand methane sources in the Arctic, Atmospheric Chem. Phys., 20, 3987–3998, https://doi.org/10.5194/acp-20-3987-2020, 2020.

Boles, J. R., Clark, J. F., Leifer, I., and Washburn, L.: Temporal variation in natural methane seep rate due to tides, Coal Oil Point area, California, J. Geophys. Res. Oceans, 106, 27077–27086, https://doi.org/10.1029/2000JC000774, 2001.

Bonaglia, S., Rütting, T., Kononets, M., Stigebrandt, A., Santos, I. R., and Hall, P. O. J.: High methane emissions from an anoxic fjord driven by mixing and oxygenation, Limnol. Oceanogr. Lett., 7, 392–400, https://doi.org/10.1002/lol2.10259, 2022.

Bryden, H. L.: New polynomials for thermal expansion, adiabatic temperature gradient and potential temperature of sea water, Deep Sea Res. Oceanogr. Abstr., 20, 401–408, https://doi.org/10.1016/0011-7471(73)90063-6, 1973.

Budkewitsch, P., Pavlic, G., Oakey, G., Jauer, C., and Decker, V.: Reconnaissance mapping of suspect oil seep occurrences in Baffin Bay and Davis Strait using satellite radar: preliminary results, Geol. Surv. Can., 7068, https://doi.org/10.4095/292280, 2013.

Castro-Morales, K., Canning, A., Arzberger, S., Overholt, W. A., Küsel, K., Kolle, O., Göckede, M., Zimov, N., and Körtzinger, A.: Highest methane concentrations in an Arctic river linked to local terrestrial inputs, Biogeosciences, 19, 5059–5077, https://doi.org/10.5194/bg-19-5059-2022, 2022.

Cramm, M. A., Neves, B. de M., Manning, C. C. M., Oldenburg, T. B. P., Archambault, P., Chakraborty, A., Cyr-Parent, A., Edinger, E. N., Jaggi, A., Mort, A., Tortell, P., and Hubert, C. R. J.: Characterization of marine microbial communities around an Arctic seabed hydrocarbon seep at Scott Inlet, Baffin Bay, Sci. Total Environ., 762, 143961, https://doi.org/10.1016/j.scitotenv.2020.143961, 2021.

~~Curry, B., Lee, C. M., and Petrie, B.: Volume, Freshwater, and Heat Fluxes through Davis Strait, 2004–05, J. Phys. Oceanogr., 41, 429–436, https://doi.org/10.1175/2010JPO4536.1, 2011.~~

Damm, E., Rudels, B., Schauer, U., Mau, S., and Dieckmann, G.: Methane excess in Arctic surface water- triggered by sea ice formation and melting, Sci. Rep., 5, 16179, https://doi.org/10.1038/srep16179, 2015.

Damm, E., Ericson, Y., and Falck, E.: Waterside convection and stratification control methane spreading in supersaturated Arctic fjords (Spitsbergen), Cont. Shelf Res., 224, 104473, https://doi.org/10.1016/j.csr.2021.104473, 2021.

Dlugokencky, E. J.: Atmospheric Methane Dry Air Mole Fractions (1983-2015) and Atmospheric Carbon Dioxide Dry Air Mole Fractions (1968-2015) from the NOAA ESRL Carbon Cycle Cooperative Global Air Sampling Network, original data files, NOAA Bremerhav., https://doi.org/10/2/co2_mm_mlo_201508_2016-08-30.zip, 2016.

Dlugokencky, E. J.: Trends in Atmospheric Methane, NOAA/GML, gml.noaa.gov/ccgg/trends_ch4/, 2022.

Dlugokencky, E. J., Crotwell, A. M., Mund, J. W., Crotwell, M. J., and Thoning, K. W.: Atmospheric Methane Dry Air Mole Fractions from the NOAA GML Carbon Cycle Cooperative Global Air Sampling Network, 1983-2020, Version 2021-07-30, https://doi.org/10.15138/VNCZ-M766, 2021.

Dølven, K. O., Ferré, B., Silyakova, A., Jansson, P., Linke, P., and Moser, M.: Autonomous methane seep site monitoring offshore western Svalbard: hourly to seasonal variability and associated oceanographic parameters, Ocean Sci., 18, 233–254, https://doi.org/10.5194/os-18-233-2022, 2022.

Fenwick, L., Capelle, D., Damm, E., Zimmermann, S., Williams, W. J., Vagle, S., and Tortell, P. D.: Methane and nitrous oxide distributions across the North American Arctic Ocean during summer, 2015, J. Geophys. Res. Oceans, 122, 390–412, https://doi.org/10.1002/2016JC012493, 2017.

Fisher, R. E., Sriskantharajah, S., Lowry, D., Lanoisellé, M., Fowler, C. M. R., James, R. H., Hermansen, O., Lund Myhre, C., Stohl, A., Greinert, J., Nisbet-Jones, P. B. R., Mienert, J., and Nisbet, E. G.: Arctic methane sources: Isotopic evidence for atmospheric inputs, Geophys. Res. Lett., 38, https://doi.org/10.1029/2011GL049319, 2011.

Fofonoff, P. and Millard, R. C. Jr.: Algorithms for computation of fundamental properties of seawater - UNESCO Digital Library, UNESCO Tech. Pap. Mar. Sci., 44, 1983.

Fratantoni, P. S. and Pickart, R. S.: The Western North Atlantic Shelfbreak Current System in Summer, J. Phys. Oceanogr., 37, 2509–2533, https://doi.org/10.1175/JPO3123.1, 2007.

Fröb, F., Olsen, A., Våge, K., Moore, G. W. K., Yashayaev, I., Jeansson, E., and Rajasakaren, B.: Irminger Sea deep convection injects oxygen and anthropogenic carbon to the ocean interior, Nat. Commun., 7, 13244, https://doi.org/10.1038/ncomms13244, 2016.

Gautier, D. L., Bird, K. J., Charpentier, R. R., Grantz, A., Houseknecht, D. W., Klett, T. R., Moore, T. E., Pitman, J. K., Schenk, C. J., Schuenemeyer, J. H., Sørensen, K., Tennyson, M. E., Valin, Z. C., and Wandrey, C. J.: Oil and gas resource potential north of the Arctic Circle, Arct. Pet. Geol., 35, https://doi.org/10.1144/M35.9, 2011.

Gregersen, U. and Bidstrup, T.: Structures and hydrocarbon prospectivity in the northern Davis Strait area, offshore West Greenland, Pet. Geosci., 14, 151–166, https://doi.org/10.1144/1354-079308-752, 2008.

Ho, D. T., Law, C. S., Smith, M. J., Schlosser, P., Harvey, M., and Hill, P.: Measurements of air-sea gas exchange at high wind speeds in the Southern Ocean: Implications for global parameterizations, Geophys. Res. Lett., 33, https://doi.org/10.1029/2006GL026817, 2006.

Hou, K. and Xu, X.: Evaluation of the Influence between Local Meteorology and Air Quality in Beijing Using Generalized Additive Models, Atmosphere, 13, 24, https://doi.org/10.3390/atmos13010024, 2022.

Hsu, S. A., Meindl, E. A., and Gilhousen, D. B.: Determining the Power-Law Wind-Profile Exponent under Near-Neutral Stability Conditions at Sea, J. Appl. Meteorol. Climatol., 33, 757–765, https://doi.org/10.1175/1520-0450(1994)033<0757:DTPLWP>2.0.CO;2, 1994.

Jähne, B., Heinz, G., and Dietrich, W.: Measurement of the diffusion coefficients of sparingly soluble gases in water, J. Geophys. Res. Oceans, 92, 10767–10776, https://doi.org/10.1029/JC092iC10p10767, 1987.

James, R. H., Bousquet, P., Bussmann, I., Haeckel, M., Kipfer, R., Leifer, I., Niemann, H., Ostrovsky, I., Piskozub, J., Rehder, G., Treude, T., Vielstädte, L., and Greinert, J.: Effects of climate change on methane emissions from seafloor sediments in the Arctic Ocean: A review, Limnol. Oceanogr., 61, S283–S299, https://doi.org/10.1002/lno.10307, 2016.

Jauer, C. D. and Budkewitsch, P.: Old marine seismic and new satellite radar data: Petroleum exploration of north west Labrador Sea, Canada, Mar. Pet. Geol., 27, 1379–1394, https://doi.org/10.1016/j.marpetgeo.2010.03.003, 2010.

~~Lamarche-Gagnon, G., Wadham, J.~~Karl, D. M., Beversdorf, L., ~~Sherwood Lollar, B., Arndt, S., Fietzek, P., Beaton, A. D., Tedstone, A. J., Telling, J., Bagshaw, E. A., Hawkings, J. R., Kohler, T. J., Zarsky, J. D., Mowlem, M. C., Anesio, A.~~Björkman, K. M., Church, M. J., Martinez, A., and ~~Stibal, M.: Greenland melt drives continuous export~~Delong, E. F.: Aerobic production of methane ~~from~~in the ~~ice sheet bed, Nature, 565, 73–77~~sea, Nat. Geosci., 1, 473–478, https://doi.org/10.1038/~~s41586-018-0800~~ngeo234, 2008.

Kvenvolden, K. A.: Methane hydrate — A major reservoir of carbon in the shallow geosphere?, Chem. Geol., 71, 41–51, https://doi.org/10.1016/0009-2541(88)90104-0, ~~2019~~1988.

Lan, X., Basu, S., Schwietzke, S., Bruhwiler, L. M. P., Dlugokencky, E. J., Michel, S. E., Sherwood, O. A., Tans, P. P., Thoning, K., Etiope, G., Zhuang, Q., Liu, L., Oh, Y., Miller, J. B., Pétron, G., Vaughn, B. H., and Crippa, M.: Improved

Constraints on Global Methane Emissions and Sinks Using δ13C-CH4, Glob. Biogeochem. Cycles, 35, e2021GB007000, https://doi.org/10.1029/2021GB007000, 2021.

Law, C. S., Nodder, S. D., Mountjoy, J. J., Marriner, A., Orpin, A., Pilditch, C. A., Franz, P., and Thompson, K.: Geological, hydrodynamic and biogeochemical variability of a New Zealand deep-water methane cold seep during an integrated three-year time-series study, Mar. Geol., 272, 189–208, https://doi.org/10.1016/j.margeo.2009.06.018, 2010.

Leifer, I. and Boles, J.: Measurement of marine hydrocarbon seep flow through fractured rock and unconsolidated sediment, Mar. Pet. Geol., 22, 551–568, https://doi.org/10.1016/j.marpetgeo.2004.10.026, 2005.

Leonte, M., Kessler, J. D., Kellermann, M. Y., Arrington, E. C., Valentine, D. L., and Sylva, S. P.: Rapid rates of aerobic methane oxidation at the feather edge of gas hydrate stability in the waters of Hudson Canyon, US Atlantic Margin, Geochim. Cosmochim. Acta, 204, 375–387, https://doi.org/10.1016/j.gca.2017.01.009, 2017.

Levy, E. M. and MacIean, B.: Natural Hydrocarbon Seepage At Scott Inlet and Buchan Gulf, Baffin Island Shelf: 1980 Update, Geol. Surv. Can., 81–1A, 401–403, https://doi.org/10.4095/109550, 1981.

Li, Y., Xie, H., Scarratt, M., Damm, E., Bourgault, D., Galbraith, P. S., and Wallace, D. W. R.: Dissolved methane in the water column of the Saguenay Fjord, Mar. Chem., 230, 103926, https://doi.org/10.1016/j.marchem.2021.103926, 2021.

Loncarevic, B. D. and Falconer, R. K. H.: An oil slick occurrence off Baffin Island, Rep. Act. Part Geol. Surv. Can. Pap., 523–524, 1977.

Manning, C. C. M~~., Preston, V. L., Jones, S. F., Michel, A. P. M., Nicholson, D. P., Duke, P. J., Ahmed, M. M. M., Manganini, K., Else, B. G. T., and Tortell, P. D.: River Inflow Dominates Methane Emissions in an Arctic Coastal System, Geophys. Res. Lett., 47, e2020GL087669, https://doi.org/10.1029/2020GL087669, 2020~~. and Nicholson, D. P.: dnicholson/gas_toolbox: MATLAB code for calculating gas fluxes, , https://doi.org/10.5281/zenodo.6126685, 2022.

Manning, C. C. M., Zheng, Z., Fenwick, L., McCulloch, R. D., Damm, E., Izett, R. W., Williams, W. J., Zimmermann, S., Vagle, S., and Tortell, P. D.: Interannual Variability in Methane and Nitrous Oxide Concentrations and Sea-Air Fluxes Across the North American Arctic Ocean (2015–2019), Glob. Biogeochem. Cycles, 36, e2021GB007185, https://doi.org/10.1029/2021GB007185, 2022.

Mau, S., Blees, J., Helmke, E., Niemann, H., and Damm, E.: Vertical distribution of methane oxidation and methanotrophic response to elevated methane concentrations in stratified waters of the Arctic fjord Storfjorden (Svalbard, Norway), Biogeosciences, 10, 6267–6278, https://doi.org/10.5194/bg-10-6267-2013, 2013.

Mau, S., Römer, M., Torres, M. E., Bussmann, I., Pape, T., Damm, E., Geprägs, P., Wintersteller, P., Hsu, C.-W., Loher, M., and Bohrmann, G.: Widespread methane seepage along the continental margin off Svalbard - from Bjørnøya to Kongsfjorden, Sci. Rep., 7, 42997, https://doi.org/10.1038/srep42997, 2017.

McGinnis, D. F., Greinert, J., Artemov, Y., Beaubien, S. E., and Wüest, A.: Fate of rising methane bubbles in stratified waters: How much methane reaches the atmosphere?, J. Geophys. Res. Oceans, 111, https://doi.org/10.1029/2005JC003183, 2006.

Melling, H., Gratton, Y., and Ingram, G.: Ocean circulation within the North Water polynya of Baffin Bay, Atmosphere-Ocean, 39, 301–325, https://doi.org/10.1080/07055900.2001.9649683, 2001.

Meredith, M., Sommerkorn, M., Cassotta, S., Derksen, C., Ekaykin, A., Hollowed, A., Kofinas, G., Mackintosh, A., Melbourne-Thomas, J., Muelbert, M. M. C., Ottersen, G., Pritchard, H., and Schuur, E. A. G.: Chapter 3: Polar regions, in:

IPCC Special Report on the Ocean and Cryosphere in a Changing Climate, Cambridge University Press, Cambridge, UK and New York, USA, 203–320, 2019.

Millero, F. J. and Poisson, A.: International one-atmosphere equation of state of seawater, Deep Sea Res. Part Oceanogr. Res. Pap., 28, 625–629, https://doi.org/10.1016/0198-0149(81)90122-9, 1981.

Neill, C., Johnson, K. M., Lewis, E., and Wallace, D. W. R.: Accurate headspace analysis of $fCO2$ in discrete water samples using batch equilibration, Limnol. Oceanogr., 42, 1774–1783, https://doi.org/10.4319/lo.1997.42.8.1774, 1997.

Nielsen, T., Laier, T., Kuijpers, A., Rasmussen, T. L., Mikkelsen, N. E., and Nørgård-Pedersen, N.: Fluid flow and methane occurrences in the Disko Bugt area offshore West Greenland: indications for gas hydrates?, Geo-Mar. Lett., 34, 511–523, https://doi.org/10.1007/s00367-014-0382-2, 2014.

Nisbet, E. G., Manning, M. R., Dlugokencky, E. J., Fisher, R. E., Lowry, D., Michel, S. E., Myhre, C. L., Platt, S. M., Allen, G., Bousquet, P., Brownlow, R., Cain, M., France, J. L., Hermansen, O., Hossaini, R., Jones, A. E., Levin, I., Manning, A. C., Myhre, G., Pyle, J. A., Vaughn, B. H., Warwick, N. J., and White, J. W. C.: Very Strong Atmospheric Methane Growth in the 4 Years 2014–2017: Implications for the Paris Agreement, Glob. Biogeochem. Cycles, 33, 318–342, https://doi.org/10.1029/2018GB006009, 2019.

Normandeau, A., MacKillop, K., Macquarrie, M., Richards, C., Bourgault, D., Campbell, D. C., Maselli, V., Philibert, G., and Clarke, J. H.: Submarine landslides triggered by iceberg collision with the seafloor, Nat. Geosci., 14, 599–605, https://doi.org/10.1038/s41561-021-00767-4, 2021.

~~Northington, R. M. and Saros, J. E.: Factors Controlling Methane in Arctic Lakes of Southwest Greenland, PLOS ONE, 11, e0159642, https://doi.org/10.1371/journal.pone.0159642, 2016.~~

Paull, C. K., Brewer, P. G., Ussler, W., Peltzer, E. T., Rehder, G., and Clague, D.: An experiment demonstrating that marine slumping is a mechanism to transfer methane from seafloor gas-hydrate deposits into the upper ocean and atmosphere, Geo-Mar. Lett., 22, 198–203, https://doi.org/10.1007/s00367-002-0113-y, 2002.

Pearce, J. L., Beringer, J., Nicholls, N., Hyndman, R. J., and Tapper, N. J.: Quantifying the influence of local meteorology on air quality using generalized additive models, Atmos. Environ., 45, 1328–1336, https://doi.org/10.1016/j.atmosenv.2010.11.051, 2011.

Platt, S. M., Eckhardt, S., Ferré, B., Fisher, R. E., Hermansen, O., Jansson, P., Lowry, D., Nisbet, E. G., Pisso, I., Schmidbauer, N., Silyakova, A., Stohl, A., Svendby, T. M., Vadakkepuliyambatta, S., Mienert, J., and Lund Myhre, C.: Methane at Svalbard and over the European Arctic Ocean, Atmospheric Chem. Phys., 18, 17207–17224, https://doi.org/10.5194/acp-18-17207-2018, 2018.

Punshon, S., Azetsu-Scott, K., and Lee, C. M.: On the distribution of dissolved methane in Davis Strait, North Atlantic Ocean, Mar. Chem., 161, 20–25, https://doi.org/10.1016/j.marchem.2014.02.004, 2014.

Punshon, S., Azetsu-Scott, K., Sherwood, O., and Edinger, E. N.: Bottom water methane sources along the high latitude eastern Canadian continental shelf and their effects on the marine carbonate system, Mar. Chem., 212, 83–95, https://doi.org/10.1016/j.marchem.2019.04.004, 2019.

Reeburgh, W. S.: Oceanic Methane Biogeochemistry, Chem. Rev., 107, 486–513, https://doi.org/10.1021/cr050362v, 2007.

Rolph, G., Stein, A., and Stunder, B.: Real-time Environmental Applications and Display sYstem: READY, Environ. Model. Softw., 95, 210–228, https://doi.org/10.1016/j.envsoft.2017.06.025, 2017.

Saunois, M., Jackson, R. B., Bousquet, P., Poulter, B., and Canadell, J. G.: The growing role of methane in anthropogenic climate change, Environ. Res. Lett., 11, 120207, https://doi.org/10.1088/1748-9326/11/12/120207, 2016.

~~Saunois, M., Stavert, A. R., Poulter, B., Bousquet, P., Canadell, J. G., Jackson, R. B., Raymond, P. A., Dlugokencky, E. J., Houweling, S., Patra, P. K., Ciais, P., Arora, V. K., Bastviken, D., Bergamaschi, P., Blake, D. R., Brailsford, G., Bruhwiler, L., Carlson, K. M., Carrol, M., Castaldi, S., Chandra, N., Crevoisier, C., Crill, P. M., Covey, K., Curry, C. L., Etiope, G., Frankenberg, C., Gedney, N., Hegglin, M. I., Höglund-Isaksson, L., Hugelius, G., Ishizawa, M., Ito, A., Janssens-Maenhout, G., Jensen, K. M., Joos, F., Kleinen, T., Krummel, P. B., Langenfelds, R. L., Laruelle, G. G., Liu, L., Machida, T., Maksyutov, S., McDonald, K. C., McNorton, J., Miller, P. A., Melton, J. R., Morino, I., Müller, J., Murguia-Flores, F., Naik, V., Niwa, Y., Noce, S., O'Doherty, S., Parker, R. J., Peng, C., Peng, S., Peters, G. P., Prigent, C., Prinn, R., Ramonet, M., Regnier, P., Riley, W. J., Rosentreter, J. A., Segers, A., Simpson, I. J., Shi, H., Smith, S. J., Steele, L. P., Thornton, B. F., Tian, H., Tohjima, Y., Tubiello, F. N., Tsuruta, A., Viovy, N., Voulgarakis, A., Weber, T. S., van Weele, M., van der Werf, G. R., Weiss, R. F., Worthy, D., Wunch, D., Yin, Y., Yoshida, Y., Zhang, W., Zhang, Z., Zhao, Y., Zheng, B., Zhu, Q., Zhu, Q., and Zhuang, Q.: The Global Methane Budget 2000–2017, Earth Syst. Sci. Data, 12, 1561–1623, https://doi.org/10.5194/essd-12-1561-2020, 2020.~~

Savitzky, Abraham. and Golay, M. J. E.: Smoothing and Differentiation of Data by Simplified Least Squares Procedures., Anal. Chem., 36, 1627–1639, https://doi.org/10.1021/ac60214a047, 1964.

Shakhova, N., Semiletov, I., Salyuk, A., Yusupov, V., Kosmach, D., and Gustafsson, Ö.: Extensive Methane Venting to the Atmosphere from Sediments of the East Siberian Arctic Shelf, Science, 327, 1246–1250, https://doi.org/10.1126/science.1182221, 2010.

Shakhova, N., Semiletov, I., Leifer, I., Sergienko, V., Salyuk, A., Kosmach, D., Chernykh, D., Stubbs, C., Nicolsky, D., Tumskoy, V., and Gustafsson, Ö.: Ebullition and storm-induced methane release from the East Siberian Arctic Shelf, Nat. Geosci., 7, 64–70, https://doi.org/10.1038/ngeo2007, 2014.

Sherwood, O. A., Davin, S. H., Lehmann, N., Buchwald, C., Edinger, E. N., Lehmann, M. F., and Kienast, M.: Stable isotope ratios in seawater nitrate reflect the influence of Pacific water along the northwest Atlantic margin, Biogeosciences, 18, 4491–4510, https://doi.org/10.5194/bg-18-4491-2021, 2021.

Silyakova, A., Jansson, P., Serov, P., Ferré, B., Pavlov, A. K., Hattermann, T., Graves, C. A., Platt, S. M., Myhre, C. L., Gründger, F., and Niemann, H.: Physical controls of dynamics of methane venting from a shallow seep area west of Svalbard, Cont. Shelf Res., 194, 104030, https://doi.org/10.1016/j.csr.2019.104030, 2020.

Stein, A. F., Draxler, R. R., Rolph, G. D., Stunder, B. J. B., Cohen, M. D., and Ngan, F.: NOAA's HYSPLIT Atmospheric Transport and Dispersion Modeling System, Bull. Am. Meteorol. Soc., 96, 2059–2077, https://doi.org/10.1175/BAMS-D-14-00110.1, 2015.

Stramma, L., Kieke, D., Rhein, M., Schott, F., Yashayaev, I., and Koltermann, K. P.: Deep water changes at the western boundary of the subpolar North Atlantic during 1996 to 2001, Deep Sea Res. Part Oceanogr. Res. Pap., 51, 1033–1056, https://doi.org/10.1016/j.dsr.2004.04.001, 2004.

Tang, C. C. L., Ross, C. K., Yao, T., Petrie, B., DeTracey, B. M., and Dunlap, E.: The circulation, water masses and sea-ice of Baffin Bay, Prog. Oceanogr., 63, 183–228, https://doi.org/10.1016/j.pocean.2004.09.005, 2004.

Thonat, T., Saunois, M., Bousquet, P., Pison, I., Tan, Z., Zhuang, Q., Crill, P. M., Thornton, B. F., Bastviken, D., Dlugokencky, E. J., Zimov, N., Laurila, T., Hatakka, J., Hermansen, O., and Worthy, D. E. J.: Detectability of Arctic methane sources at six sites performing continuous atmospheric measurements, Atmospheric Chem. Phys., 17, 8371–8394, https://doi.org/10.5194/acp-17-8371-2017, 2017.

Thornton, B. F., Geibel, M. C., Crill, P. M., Humborg, C., and Mörth, C.-M.: Methane fluxes from the sea to the atmosphere across the Siberian shelf seas, Geophys. Res. Lett., 43, 5869–5877, https://doi.org/10.1002/2016GL068977, 2016.

Thornton, B. F., Prytherch, J., Andersson, K., Brooks, I. M., Salisbury, D., Tjernström, M., and Crill, P. M.: Shipborne eddy covariance observations of methane fluxes constrain Arctic sea emissions, Sci. Adv., 6, https://doi.org/10.1126/sciadv.aay7934, 2020.

Wanninkhof, R.: Relationship between wind speed and gas exchange over the ocean revisited, Limnol. Oceanogr. Methods, 12, 351–362, https://doi.org/10.4319/lom.2014.12.351, 2014.

Wiesenburg, D. A. and Guinasso, N. L. Jr.: Equilibrium Solubilities of Methane, Carbon Monoxide, and Hydrogen in Water and Sea Water, J. Chem. Eng. Data, 24, https://doi.org/10.1021/je60083a006, 1979.

Wood, S. N.: Fast stable restricted maximum likelihood and marginal likelihood estimation of semiparametric generalized linear models., J. R. Stat. Soc., 73, 3–36, 2011.

Wu, Y. S., Hannah, C. G., Petrie, B., Pettipas, R., Peterson, I., Prinsenberg, S., Lee, C., and Moritz, R.: Ocean current and sea ice statistics for Davis Strait, Fisheries and Oceans Canada, 2013.

Zhao, Y., Booge, D., Marandino, C. A., Schlundt, C., Bracher, A., Atlas, E. L., Williams, J., and Bange, H. W.: Dimethylated sulfur compounds in the Peruvian upwelling system, Biogeosciences, 19, 701–714, https://doi.org/10.5194/bg-19-701-2022, 2022.